It has recently been shown that marmosets, another member of New World monkeys, are susceptible to GBV-B infection and develop relatively lower levels of acute viremia (10^5–10^8 copies/ml) as compared with that in tamarins (10^7–10^{10} copies/ml) (Lanford et al., 2003; Bright et al., 2004; Woollard et al., 2008; Weatherford et al., 2009), although it remains elusive whether the marmosets could permit persistent GBV-B infection. Considering that the viral loads in the acute phase of experimental HCV infection of chimpanzees that consequently develop persistent infection are generally 10^7 copies/ml or less (Fernandez et al., 2004; Bukh et al., 2008), it is possible that the lower viral loads in the acute phase is preferable for the establishment of viral persistency. We thus initiated studies of the dynamics of viral and immunological status following GBV-B infection of tamarins and marmosets in a longitudinal follow-up study. We show here for the first time that GBV-B infection produces a chronic and progressive hepatitis C-like disease in marmosets as demonstrated by fibrosis and a recurrent ALT increase and that one of the marmosets experienced acute exacerbation of chronic hepatitis as indicated by piecemeal necrosis and an ALT flare >4 years after infection.

MATERIALS AND METHODS

ANIMALS

Adult red-handed tamarins (*Saguinus midas*) and common marmosets (*Callithrix jacchus*) were housed in individual cages at the Tsukuba Primate Research Center. All animal studies were conducted in accordance with the protocols of experimental procedures that were approved by the Animal Welfare and Animal Care Committees of the National Institute of Biomedical Innovation and the National Institute of Infectious Diseases.

GBV-B INFECTION IN TAMARINS AND MARMOSETS

GBV-B infectious serum obtained from a tamarin (1.3×10^9 viral RNA copies per inoculum) was injected into each tamarin and marmoset intrahepatically as previously described (Ishii et al., 2007). We confirmed that the inoculum contained no mutations as compared with the original sequence. Of note, an anti-luciferase siRNA in a cationic liposome formulation was administered to one of the marmosets (Cj05-002) 2 days before the infection, which was performed as previously described (Yokota et al., 2007). Blood samples were periodically collected from the femoral vein of each animal under anesthesia and the plasma samples were evaluated for GBV-B genomic RNA, ALT, and antibodies against GBV-B core and NS3 proteins.

QUANTIFICATION OF GBV-B GENOMIC RNA

GBV-B RNA was isolated from the plasma samples by using a QIAamp MinElute Virus Spin kit (QIAGEN) and was quantified by real-time PCR using the 5′-exonuclease PCR (TaqMan) assay system (Ishii et al., 2007). The primers 558F [5′-AACGAGCAAAGCGCAAAGTC] and 626R [5′-CATCATGGATACCAGCAATTTTGT] and the probe 579P [5′-FAM-AGCGCGATGCTCGGCCTCGTA-TAMRA] (Beames et al., 2000) were obtained from Sigma-Aldrich. The cutoff value was 10^3 copies/ml. All the specimens were evaluated in duplicate and the average values were calculated.

DETECTION OF ANTIBODIES AGAINST GBV-B CORE AND NS3 PROTEINS BY ELISA

Tamarin and marmoset plasma samples were evaluated for anti-GBV-B core and NS3 antibodies by ELISA as described previously (Ishii et al., 2007).

HISTOPATHOLOGICAL AND IMMUNOHISTOCHEMICAL ANALYSES

Liver samples obtained by necropsy from the GBV-B-infected marmoset were examined histopathologically as previously described (Ishii et al., 2007). For standard histological examination, the sections were subjected to hematoxylin and eosin (HE) staining. Masson's trichrome staining was also performed to estimate the development of fibrosis according to a standard laboratory protocol. To detect the viral protein in tissues, we employed a mouse anti-core monoclonal antibody, 5A10, that we generated. In brief, Mice were immunized with the GBV-B core protein expressed in *E. coli* (Ishii et al., 2007). Hybridoma cells producing an anti-core mAb were screened by both the core-expressing 293T cells and the liver sections of an acutely GBV-B-infected tamarin. Liver samples were fixed in 10% neutral buffered formalin and embedded in paraffin wax. Sections were deparaffinized by pretreating with 0.5% periodic acid and then subjected to antigen retrieval with citric acid buffer and heating in an autoclave for 10 min at 121°C. The sections were then incubated free floating in primary antibody solution (5A10; 1:50 dilution) overnight at 4°C. Following brief washes with wash buffer, the sections were sequentially incubated with a biotinylated goat anti-mouse IgG (1:400 dilution), followed by addition of a streptavidin–biotin–horseradish peroxidase complex (sABC kit; DAKO, Denmark). Immunoreactive elements in the sections were visualized by treatment with 3,3′-diaminobenzidine tetroxide (Dojin Kagaku, Japan), together with counterstaining with hematoxylin.

DETERMINATION OF THE GBV-B SEQUENCE

Viral RNA was isolated from the plasma of GBV-B-infected marmosets as described above. GBV-B cDNA was synthesized using SuperScript reverse transcriptase III (Invitrogen) with random hexamer primers (Invitrogen). The resulting cDNAs were used to obtain PCR amplification products of lengths of 0.5–1.0 kb, using GBV-B-specific primers and LA-Taq DNA polymerase (TaKaRa). The PCR products were then purified from the gel using a QIA-quick gel extraction kit (QIAGEN), and the purified amplimers were sequenced directly using a CEQ-2000XL analysis system (Beckman) with a DTCS quick start kit and GBV-B-specific primers according to the manufacturer's instructions. Sequence data were analyzed using the Sequencher 4.8 (Gene Codes) and Mac Vector 10.6 (MacVector) software packages. The GenBank accession numbers of the viral genome sequences in each time point are as follows: AB630358, AB630359, and AB630360 for 45, 104, and 135 weeks after infection in Cj05-002; AB630361, AB630362, AB630363, and AB630364 for 33, 88, 141, and 229 weeks after infection in Cj05-004, respectively. Throughout this article, the amino acids are numbered according to the full-length genome sequence of isolate pGBB (GenBank accession number AF179612).

RESULTS

GBV-B INFECTION IN TAMARINS AND MARMOSETS

Four tamarins and four marmosets were intrahepatically inoculated with GBV-B and the growth kinetics and pathogenesis of the virus were compared. In tamarins, the peak viral loads in plasma reached 10^9–10^{10} copies/ml in the acute phase and the viremia was maintained for an average of 3 months in parallel with increases in plasma ALT levels (**Figure 1A**). Antibodies reactive with the viral core and NS3 proteins were developed in all of the tamarins as the plasma viral loads were reduced and the antibody titers reached maximum levels concurrently with the complete loss of detectable viral RNA (**Figure 1A**). In contrast, two of four marmosets infected with GBV-B developed chronic infection while the others exhibited a phenotype similar to that of the tamarins (i.e., subacute clearance of the viremia followed by antibody responses). One exception is that lower plasma viral loads (10^7–10^8 copies/ml) were observed in the marmosets relative to those of the tamarins (**Figure 1B**). The details of the chronically infected marmosets are described below.

Case 1: Cj05-002 (**Figures 1B** and **2**). The viral RNA was undetectable until week 4 post infection (p.i.) and then gradually increased to a peak at week 18 p.i. (3×10^7 copies/ml). Subsequently, this case retained intermittent viremia during the observation period of week 180 p.i., while the intervals between the viremia phases were prolonged. Importantly, the titers of anti-core and anti-NS3 antibodies reached a persistent plateau at 6 months and 1 year p.i., respectively. In addition, ALT levels were recurrently increased without observation of other clinical symptoms.

Case 2: Cj05-004 (**Figures 1B** and **2**). During the acute phase of infection, the level of viremia was relatively low and transient, followed by a 1-year period when the virus was essentially undetectable. Irrespective of the very low viral load, the titer of anti-NS3 but not anti-core antibody steadily increased and reached a plateau at week 42 p.i. Moreover, an occasional but obvious increase in the level of ALT was observed during this period. We thus suspected that antigenic stimulation by a lower level of viral growth in the liver, which remained below detectable levels in blood, might lead to the induction of the anti-NS3 antibody and the recurrent ALT increase. Subsequently, viremia became detectable at week 58 p.i. and 10^4–10^5 copies/ml of the viral RNA persisted until week 108 p.i. Thereafter, an abrupt increase of the anti-core antibody was detected, concomitant with augmentation of the viral load of $10^{5.5}$ copies/ml on average and recurrent increases in the ALT level. Eventually, the individual was euthanized at week 229 p.i. because of poor prognosis since the ALT value drastically increased by 161-fold, which was accompanied by a dramatic decrease of platelet counts and a deteriorating general status. Histopathological analyses of the necropsy samples demonstrated that the liver developed diffuse piecemeal necrosis with infiltration of lymphocytes and

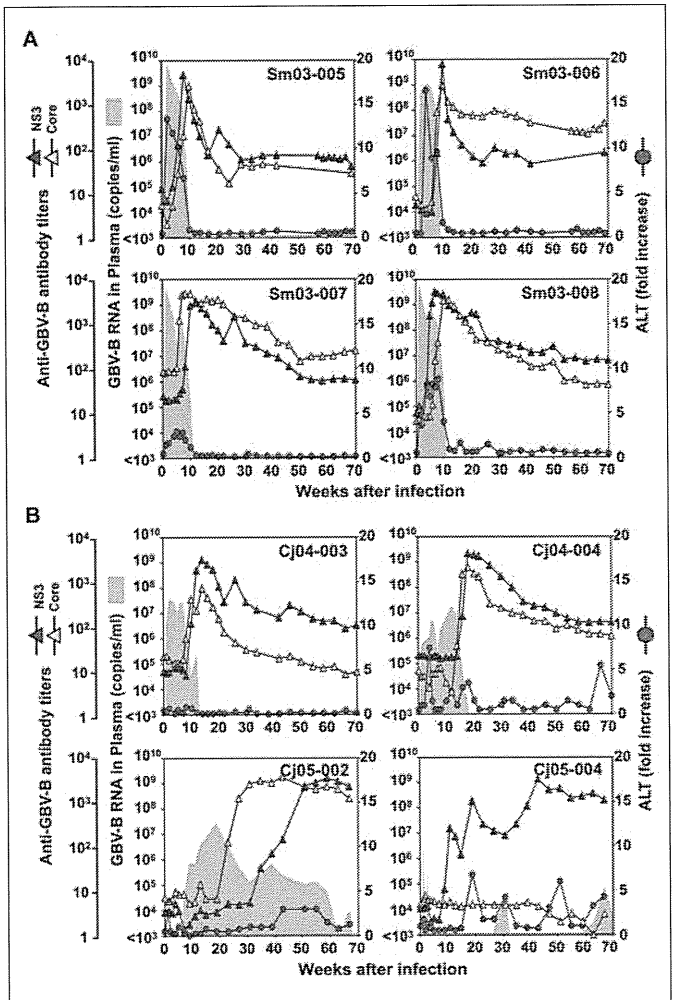

FIGURE 1 | Infection profiles until week 70 p.i. of tamarins (A) and marmosets (B) inoculated intrahepatically with GBV-B infectious serum obtained from a tamarin. Plasma samples periodically obtained from the monkeys were evaluated for the copy numbers of GBV-B genomic RNA (green shaded area), ALT levels (red circles), and the antibody titers against GBV-B core and NS3 (blue and yellow triangles, respectively).

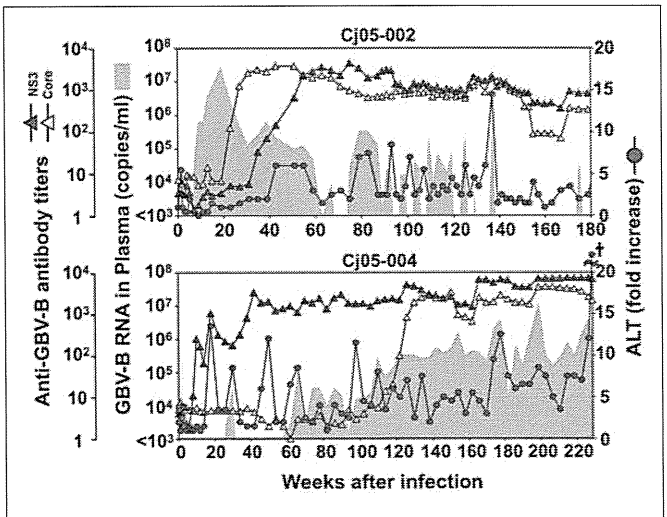

FIGURE 2 | Profiles of the marmosets persistently infected with GBV-B. Plasma samples periodically obtained from the marmosets were evaluated for the copy numbers of GBV-B genomic RNA (green shaded area), ALT levels (red circles), and the antibody titers against GBV-B core and NS3 (blue and yellow triangles, respectively). The cruciate mark in Cj05-004 indicates that the individual was euthanized due to a poor prognosis at week 229 p.i. At that time, the ALT value in plasma had increased by 161-fold.

formation of lymphoid follicles (**Figure 3A**, Appendix). The viral load in the liver was relatively high (3.8×10^4 copies/mg tissue weight), which was similar to the viral load observed for tamarins acutely infected with GBV-B (Ishii et al., 2007). The high viral load in the liver was consistent with a large number of granular positive signals for the core protein, which was in similar manner with the core protein of HCV (Miyanari et al., 2007), as immunostained with an anti-GBV-B core monoclonal antibody (**Figure 3B**). Notably, Masson trichrome staining (**Figures 3C,D**) as well as Elastica van Gieson staining (Appendix) demonstrated that the liver also developed diffuse and abundant fibrosis. The disease of this marmoset was therefore diagnosed as a case of acute exacerbation of progressive chronic hepatitis by GBV-B infection.

ANALYSIS OF MUTATIONS IN GBV-B GENOMES

Next, we determined the dominant sequence of the viral genomes at weeks 45, 104, and 135 p.i. in Cj05-002 and weeks 33, 88, 141, and 229 p.i. in Cj05-004. As seen in **Figure 4A**, it was found that there was no specific region in which extensive nucleotide mutations occurred throughout the study periods and that the nucleotide mutation rates were $1.9–2.9 \times 10^{-3}$ and $1.5–3.6 \times 10^{-3}$ changes per site per year in Cj05-002 and Cj05-004, respectively (**Table 1**). In terms of amino acid substitution, we observed the following: (i) several back or sequential mutations (G250V > A, S731L > S, E2346G > E in Cj05-002; V254A > V, I285V > I, L495S > L, T735A > T, F2135L > F > S in Cj05-004) in both marmosets; (ii) highly selective non-synonymous mutations that were remarkable in E1, but such mutations were rarely observed in core (**Figures 4** and **5**); and (iii) the non-synonymous mutation rates were $1.8–4.0 \times 10^{-3}$ and $2.1–4.6 \times 10^{-3}$ substitutions per site per year in Cj05-002 and Cj05-004, respectively (**Figures 4** and **5; Table 2**). (iv) The non-synonymous changes detected mainly in NS5A and NS5B in both animals were also observed in a number of previous reports (Simons et al., 1995; Bukh et al., 1999; Sbardellati et al., 2001; Martin et al., 2003; Nam et al., 2004; Kyuregyan et al., 2005; Weatherford et al., 2009; Takikawa et al., 2010). It may be reasonable to consider that the molecular clone we employed (Bukh et al., 1999) was derived from a minor clone of mixed populations and emergence of a new mutations easily occurred as a mechanism of GBV-B adaptation to a new host, while it is also possible that "consensus" non-synonymous changes were due to either a result of a selection of the pre-existent minor variants. Taken together, these results suggest that efficient

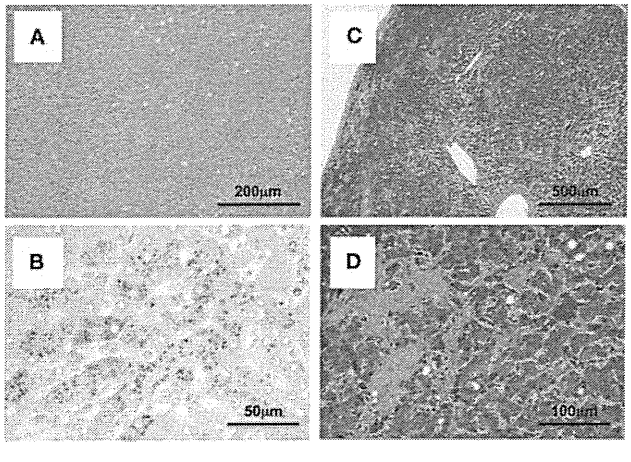

FIGURE 3 | Histopathological and immunohistochemical analyses of the liver from Cj05-004 at week 229 p.i. HE staining (A), immunohistochemical staining for the core protein of GBV-B (B), and Masson's trichrome staining (C,D) are shown.

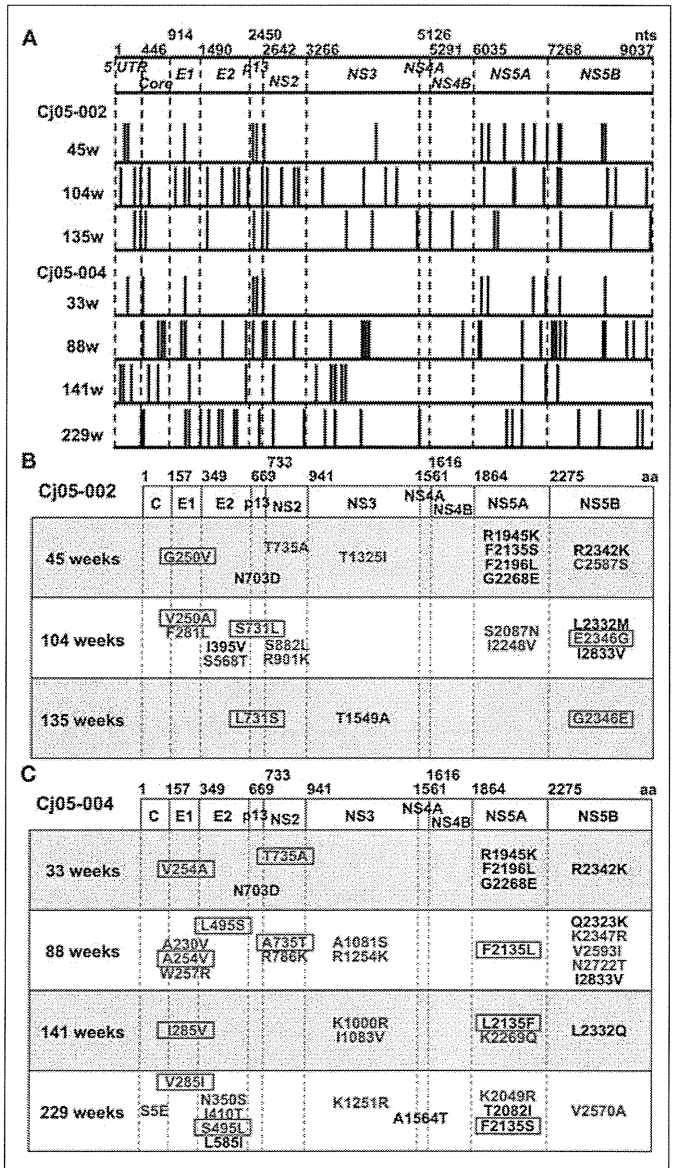

FIGURE 4 | Mutations in the viral genome sequences amplified from plasma of the marmosets persistently infected with GBV-B. (A) Positions of the nucleotide mutations in the viral genome sequences at multiple time points (at weeks 45, 104, and 135 in Cj05-002 and weeks 33, 88, 141, and 229 in Cj05-004) are illustrated as bars. **(B,C)** Positions of the non-synonymous mutations in the viral genome sequences at multiple time points are shown. **(B)** Cj05-002; **(C)** Cj05-004. Positions of the mutations that had been identified in previous reports are indicated as black, while those unidentified previously are shown as blue. Red squares illustrate back or sequential mutations.

Table 1 | Summary of the nucleotide substitutions in GBV-B genome sequences amplified from plasma of the marmosets persistently infected with GBV-B.

Genomic region	nt position	No. (%) of nt differences						
		Cj05-002			Cj05-004			
		45 weeks	104 weeks	135 weeks	33 weeks	88 weeks	141 weeks	229 weeks
5'UTR	1–445	2 (0.45)	3 (0.67)	2 (0.45)	1 (0.22)	0 (0)	3 (0.67)	0 (0)
Core	446–913	0 (0)	1 (0.21)	1 (0.21)	1 (0.21)	4 (0.85)	2 (0.43)	3 (0.64)
E1	914–1489	1 (0.17)	3 (0.52)	0 (0)	1 (0.17)	3 (0.52)	1 (0.17)	2 (0.35)
E2	1490–2449	0 (0)	5 (0.52)	1 (0.10)	0 (0)	2 (0.21)	1 (0.10)	6 (0.63)
p13	2450–2641	2 (1.04)	1 (0.52)	2 (1.04)	2 (1.04)	1 (0.52)	0 (0)	1 (0.52)
NS2	2642–3265	1 (0.16)	5 (0.80)	1 (0.16)	1 (0.16)	4 (0.64)	1 (0.16)	2 (0.32)
NS3	3266–5125	1 (0.05)	4 (0.22)	3 (0.16)	0 (0)	5 (0.27)	6 (0.32)	3 (0.16)
NS4A	5126–5290	0 (0)	0 (0)	0 (0)	0 (0)	0 (0)	0 (0)	1 (0.61)
NS4B	5291–6034	0 (0)	0 (0)	2 (0.27)	0 (0)	1 (0.13)	0 (0)	0 (0)
NS5A	6035–7267	6 (0.49)	4 (0.32)	2 (0.16)	4 (0.32)	4 (0.32)	2 (0.16)	3 (0.24)
NS5B	7268–9037	4 (0.23)	5 (0.28)	3 (0.17)	2 (0.11)	10 (0.56)	1 (0.06)	4 (0.23)
Total	9037	17 (0.19)	31 (0.34)	17 (0.19)	12 (0.13)	34 (0.38)	17 (0.19)	25 (0.28)
Mutation rate/year		2.2×10^{-3}	3.0×10^{-3}	3.2×10^{-3}	2.1×10^{-3}	3.6×10^{-3}	1.8×10^{-3}	1.6×10^{-3}

Table 2 | Summary of the amino acid substitutions in GBV-B genome sequences amplified from plasma of the marmosets persistently infected with GBV-B.

Amino acid region	aa position	No. (%) of aa differences						
		Cj05-002			Cj05-004			
		45 weeks	104 weeks	135 weeks	33 weeks	88 weeks	141 weeks	229 weeks
Core	1–156	0 (0)	0 (0)	0 (0)	0 (0)	0 (0)	0 (0)	1 (0.64)
E1	157–348	1 (0.52)	2 (1.04)	0 (0)	1 (0.52)	3 (1.56)	1 (0.52)	1 (0.52)
E2	349–613	0 (0)	2 (0.63)	0 (0)	0 (0)	1 (0.31)	0 (0)	4 (1.25)
P13	669–732	1 (1.56)	1 (1.56)	1 (1.56)	1 (1.56)	0 (0)	0 (0)	0 (0)
NS2	733–940	1 (0.48)	2 (0.96)	0 (0)	1 (0.48)	2 (0.96)	0 (0)	0 (0)
NS3	941–1560	1 (0.16)	0 (0)	1 (0.16)	0 (0)	2 (0.32)	2 (0.32)	1 (0.16)
NS4A	1561–1615	0 (0)	0 (0)	0 (0)	0 (0)	0 (0)	0 (0)	1 (1.82)
NS4B	1616–1863	0 (0)	0 (0)	0 (0)	0 (0)	0 (0)	0 (0)	0 (0)
NS5A	1864–2274	4 (0.97)	2 (0.49)	0 (0)	3 (0.73)	1 (0.24)	2 (0.49)	3 (0.73)
NS5B	2275–2864	2 (0.34)	3 (0.51)	1 (0.17)	1 (0.17)	5 (0.85)	1 (0.17)	1 (0.17)
Total	2864	10 (0.38)	12 (0.42)	3 (0.10)	7 (0.24)	14 (0.49)	6 (0.21)	12 (0.42)
Mutation rate/year		4.0×10^{-3}	3.7×10^{-3}	1.8×10^{-3}	3.9×10^{-3}	4.6×10^{-3}	2.1×10^{-3}	2.5×10^{-3}

and selective evasion from immune pressure in the two marmosets resulted in long-term persistent GBV-B infection accompanied by subsequent chronic hepatitis.

DISCUSSION

In this study, we show for the first time that GBV-B is capable of eliciting a chronic and progressive hepatitis C-like disease in marmosets. Evidence for this condition is demonstrated by long-term persistent GBV-B infection, recurrent ALT increase, and fibrosis. Moreover, one of the chronically infected marmosets developed acute exacerbation of chronic hepatitis as indicated by diffuse piecemeal liver necrosis and an ALT flare, which is seen in patients with viral hepatitis (Perrillo, 1997). While the usefulness of the monkey model as a surrogate model for HCV infection has been under debate due to the virtual inability of GBV-B to cause chronic hepatitis C-like disease in tamarins, the present data demonstrate that the ability of GBV-B to induce the chronic disease is likely to be inherent depending on the differences between species and individuals.

It has been reported that tamarins generally permit extensive replication of GBV-B in the subacute phase of infection and develop acute hepatitis as shown by significant increases of serum enzymes such as ALT and isocitrate dehydrogenase. The viral load in marmosets seems to be lower than in tamarins (Lanford et al.,

2003; Bright et al., 2004; Woollard et al., 2008; Weatherford et al., 2009). A recent report indicated that marmosets exhibit susceptible and partially resistant phenotypes upon infection with GBV-B (Weatherford et al., 2009). Consistent with this finding, the present results also showed that the marmosets appeared to exhibit two phenotypes (**Figure 1B**). Importantly, the long-term persistent GBV-B infection was established in the marmosets with lower viral loads during the initial weeks p.i. (**Figure 1B**; Cj05-002 and Cj05-004). This suggests that the mild viral growth in the marmosets with a "partially resistant" phenotype is critical for the establishment of the chronic infection. Of note, the viral growth was undetectable until week 6 p.i. in Cj05-002, owing to unexpected interferon responses that were induced by administration of an anti-luciferase small interfering RNA in a cationic liposome formulation 2 days before GBV-B infection (Yokota et al., 2007). Irrespective of the partial suppression of the viral growth, humoral immune responses were delayed and consequently the individual developed chronic infection. Taken together, it is reasonable to assume that the viral persistence in marmosets may be closely associated with inefficient antiviral immune responses that are elicited at the periods of the lower viral loads. Previously, we and others employed relatively higher amounts of GBV-B for challenge in tamarins and marmosets. This could result in greater viral loads in the acute phase than those in humans and chimpanzees infected with HCV, followed by induction of efficient protective immunity and acute clearance. To clarify the mechanisms by which chronic GBV-B infection is established, further characterization of the differences in innate and acquired antiviral immunity between individuals with acute clearance and chronic infection will be needed.

Accumulating evidence suggests that escape mutations occurring during the course of chronic HCV infection may lead to evasion of humoral and cellular antiviral immunity (Bowen and Walker, 2005a,b; Burke and Cox, 2010). Consistent with these observations, we found that GBV-B acquired multiple back or sequential non-synonymous mutations (e.g., G250V > A, S731L > S, E2346G > E in Cj05-002; and V254A > V, I285V > I, L495S > L, T735A > T, F2135L > F > S in Cj05-004) in the chronically infected marmosets. Highly selective non-synonymous mutations were identified especially in E1, but such mutations were rarely observed in core (**Figures 4** and **5**). Moreover, the non-synonymous mutations in the E1 and NS3 regions occurred throughout the observation periods in Cj05-004 with chronic GBV-B infection, which had not been identified previously (Simons et al., 1995; Bukh et al., 1999; Sbardellati et al., 2001; Martin et al., 2003; Nam et al., 2004; Kyuregyan et al., 2005; Weatherford et al., 2009; Takikawa et al., 2010). Together with the finding that the rates of both synonymous and non-synonymous mutations were similar to those observed in cases of HCV (Ogata et al., 1991; Fernandez et al., 2004), these results strongly suggest that efficient and selective evasion from immune pressures may result in long-term persistent GBV-B infection and subsequent chronic hepatitis. Further analyses on the functional significance of the non-synonymous mutations will clarify this possibility.

It is surprising that in Cj05-004, the antibody titer to NS3 was observed to steadily increase after week 10 p.i. irrespective of the scarce viral loads over 1 year p.i., including the bipartite

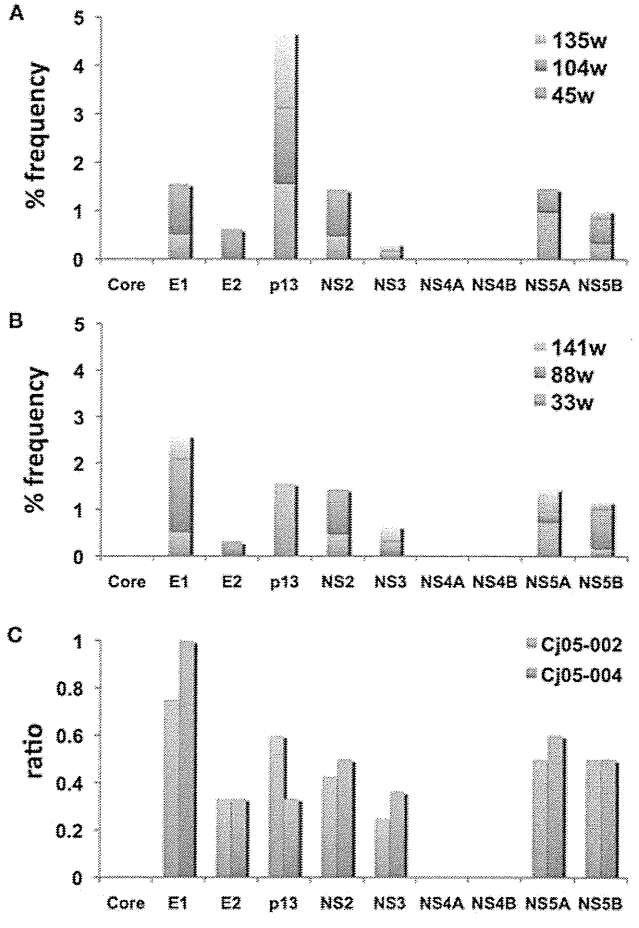

FIGURE 5 | The frequency of the non-synonymous mutations in the viral genome sequences amplified from plasma of the marmosets persistently infected with GBV-B. (A,B) The accumulated frequency of the non-synonymous mutations per total amino acid numbers of each viral protein at multiple time points are illustrated [**(A)** at weeks 45, 104, and 135 in Cj05-002; **(B)** weeks 33, 88, and 141 in Cj05-004]. To compare the frequency between the two marmosets, the data at week 229 p.i. in Cj05-004 are omitted. **(C)** The ratio of the non-synonymous mutations per total numbers of nucleotide mutations identified at weeks 45, 104, and 135 in Cj05-002 and at weeks 33, 88, and 141 in Cj05-004 in each viral gene. To compare the frequency between the two marmosets, the data at week 229 p.i. in Cj05-004 are omitted.

periods of weeks 4–26 and 34–58 p.i. when the virus was undetectable (**Figure 1**). Considering that three spikes of ALT levels were observed during these periods, our results suggest that antigenic stimulation by the lower level of viral growth in the liver, which was below detectable levels in blood, may induce the antibody and cytotoxic T-cell responses. In addition, during longitudinal analyses of monkeys experimentally infected with GBV-B, it is important to comprehensively evaluate multiple parameters, including viral loads, serum enzymes, and antibodies against core and NS3 proteins, to define whether virus-infected monkeys that produce no detectable viremia for a period of time have cleared the virus or are experiencing a latent period of chronic infection.

ACKNOWLEDGMENTS

We wish to thank T. Kurosawa, M. Fujita, and T. Ikoma for their helpful assistance and the members of Corporation for Production and Research of Laboratory Primates for technical assistance. Financial support: This work was supported by grants from the Ministry of Health, Labor, and Welfare of Japan (to Hirofumi Akari).

REFERENCES

Akari, H., Iwasaki, Y., Yoshida, T., and Iijima, S. (2009). Non-human primate surrogate model of hepatitis C virus infection. *Microbiol. Immunol.* 53, 53–57.

Beames, B., Chavez, D., Guerra, B., Notvall, L., Brasky, K. M., and Lanford, R. E. (2000). Development of a primary tamarin hepatocyte culture system for GB virus-B: a surrogate model for hepatitis C virus. *J. Virol.* 74, 11764–11772.

Beames, B., Chavez, D., and Lanford, R. E. (2001). GB virus B as a model for hepatitis C virus. *ILAR J.* 42, 152–160.

Boonstra, A., van der Laan, L. J., Vanwolleghem, T., and Janssen, H. L. (2009). Experimental models for hepatitis C viral infection. *Hepatology* 50, 1646–1655.

Bowen, D. G., and Walker, C. M. (2005a). Mutational escape from CD8+ T cell immunity: HCV evolution, from chimpanzees to man. *J. Exp. Med.* 201, 1709–1714.

Bowen, D. G., and Walker, C. M. (2005b). Adaptive immune responses in acute and chronic hepatitis C virus infection. *Nature* 436, 946–952.

Bright, H., Carroll, A. R., Watts, P. A., and Fenton, R. J. (2004). Development of a GB virus B marmoset model and its validation with a novel series of hepatitis C virus NS3 protease inhibitors. *J. Virol.* 78, 2062–2071.

Bukh, J. (2004). A critical role for chimpanzee model in the study of hepatitis C. *Hepatology* 39, 1469–1475.

Bukh, J., Apgar, C. L., and Yanagi, M. (1999). Toward a surrogate model for hepatitis C virus: An infectious molecular clone of the GB virus-B hepatitis agent. *Virology* 262, 470–478.

Bukh, J., Thimme, R., Meunier, J. C., Faulk, K., Spangenberg, H. C., Chang, K. M., Satterfield, W., Chisari, F. V., and Purcell, R. H. (2008). Previously infected chimpanzees are not consistently protected against reinfection or persistent infection after reexposure to the identical hepatitis C virus strain. *J. Virol.* 82, 8183–8195.

Burke, K. P., and Cox, A. L. (2010). Hepatitis C virus evasion of adaptive immune responses: a model for viral persistence. *Immunol. Res.* 47, 216–227.

Chisari, F. V. (2005). Unscrambling hepatitis C virus-host interactions. *Nature* 436, 930–932.

Feld, J. J., and Hoofnagle, J. H. (2005). Mechanism of action of interferon and ribavirin in treatment of hepatitis C. *Nature* 436, 967–972.

Fernandez, J., Taylor, D., Morhardt, D. R., Mihalik, K., Puig, M., Rice, C. M., Feinstone, S. M., and Major, M. E. (2004). Long-term persistence of infection in chimpanzees inoculated with an infectious hepatitis C virus clone is associated with a decrease in the viral amino acid substitution rate and low levels of heterogeneity. *J. Virol.* 78, 9782–9789.

Hoofnagle, J. H. (1997). Hepatitis C: the clinical spectrum of disease. *Hepatology* 26, 15S–20S.

Ishii, K., Iijima, S., Kimura, N., Lee, Y. J., Ageyama, N., Yagi, S., Yamaguchi, K., Maki, N., Mori, K., Yoshizaki, S, Machida, S., Suzuki, T., Iwata, N., Sata, T., Terao, K., Miyamura, T., and Akari, H. (2007). GBV-B as a pleiotropic virus: distribution of GBV-B in extrahepatic tissues in vivo. *Microbes Infect.* 9, 515–521.

Jacob, J. R., Lin, K. C., Tennant, B. C., and Mansfield, K. G. (2004). GB virus B infection of the common marmoset (*Callithrix jacchus*) and associated liver pathology. *J. Gen. Virol.* 85, 2525–2533.

Kyuregyan, K. K., Poleschuk, V. F., Zamyatina, N. A., Isaeva, O. V., Michailov, M. I., Ross, S., Bukh, J., Roggendorf, M., and Viazov, S. (2005). Acute GB virus B infection of marmosets is accompanied by mutations in the NS5A protein. *Virus Res.* 114, 154–157.

Lanford, R. E., Chavez, D., Notvall, L., and Brasky, K. M. (2003). Comparison of tamarins and marmosets as hosts for GBV-B infections and the effect of immunosuppression on duration of viremia. *Virology* 311, 72–80.

Lavanchy, D. (2009). The global burden of hepatitis C. *Liver Int.* 29, 74–81.

Martin, A., Bodola, F., Sanger, D. V., Goettge, K., Popov, V., Rijnbrand, R., Lanford, R. E., and Lemon, S. M. (2003). Chronic hepatitis associated with GB virus B persistence in a tamarin after intrahepatic inoculation of synthetic viral RNA. *Proc. Natl. Acad. Sci. U.S.A.* 100, 9962–9967.

Melnikova, I. (2008). Hepatitis C therapies. *Nat. Rev. Immunol.* 5, 799–800.

Miyanari, Y., Atsuzawa, K., Usuda, N., Watashi, K., Hishiki, T., Zayas, M., Bartenschlager, R., Wakita, T., Hijikata, M., and Shimotohno, K. (2007). The lipid droplet is an important organelle for hepatitis C virus production. *Nat. Cell Biol.* 9, 1089–1097.

Muerhoff, A. S., Leary, T. P., Simons, J. N., Pilot-Matias, T. J., Dawason, G. J., Erker, J. C., Chalmers, M. L., Schlauder, G. G., Desai, S. M., and Mushahwer, I. K. (1995). Genomic organization of GB viruses A and B: two new members of the Flaviviridae associated with GB agent hepatitis. *J. Virol.* 69, 5621–5630.

Nam, J. H., Faulk, K., Engle, R. E., Govindarajan, S., St. Claire, M., and Bukh, J. (2004). In vivo analysis of the 3′ untranslated region of GB virus B after in vitro mutagenesis of an infections cDNA clone: persistent infection in a transfected tamarin. *J. Virol.* 78, 9389–9399.

Ogata, N., Alter, H. J., Miller, R. H., and Purcell, R. H. (1991). Nucleotide sequence and mutation rate of the H strain of hepatitis C virus. *Proc. Natl. Acad. Sci. U.S.A.* 88, 3392–3396.

Ohba, K., Mizokami, M., Lau, J. Y., Orito, E., Ikeo, K., and Gojobori, T. (1996). Evolutionary relationship of hepatitis C, pesti-, flavi-, plantviruses, and newly discovered GB hepatitis agents. *FEBS Lett.* 378, 232–234.

Perrillo, R. P. (1997). The role of liver biopsy in hepatitis C. *Hepatology* 26, 57S–61S.

Rehermann, B., and Nascimbeni, M. (2005). Immunology of hepatitis B virus and hepatitis C virus infection. *Nat. Rev. Immunol.* 5, 215–229.

Sbardellati, A., Scarselli, E., Verschoor, E., De Tomassi, A., Lazzaro, D., and Traboni, C. (2001). Generation of infectious and transmissible virions from a GB virus B full-length consensus clone in tamarins. *J. Gen. Virol.* 82, 2437–2448.

Seeff, L. B., and Hoofnagle, J. H. (2002). National Institutes of Health Consensus Development Conference: management of hepatitis C: 2002. *Hepatology* 36, S1–S2.

Simons, J. N., Pilot-Matias, T. J., Leary, T. P., Dawason, G. J., Desai, S. M., Schlauder, G. G., Muerhoff, A. S., Erker, J. C., Buijk, S. L., Chalmers, M. L., Van Sant, C. L., and Mushahwar, I. K. (1995). Identification of two *Flavivirus*-like genomes in the GB hepatitis agent. *Proc. Natl. Acad. Sci. U.S.A.* 92, 3401–3405.

Takikawa, S., Engle, R. E., Faulk, K. N., Emerson, S. U., Purcell, R. H., and Bukh, J. (2010). Molecular evolution of GB virus B hepatitis virus during acute resolving and persistent infections in experimentally infected tamarins. *J. Gen. Virol.* 91, 727–733.

Weatherford, T., Chavez, D., Brasky, K. M., and Lanford, R. E. (2009). The marmoset model of GB virus B infections: adaptation to host phenotypic variation. *J. Virol.* 83, 5806–5814.

Woollard, D. J., Haqshenas, G., Dong, X., Pratt, B. F., Kent, S. J., and Gowans, E. J. (2008). Virus-specific T-cell immunity correlates with control of GB virus B infection in marmosets. *J. Virol.* 82, 3054–3060.

Yokota, T., Iijima, S., Kubodera, T., Ishii, K., Katakai, Y., Ageyama, N., Chen, Y., Lee, Y. J., Unno, T., Nishina, K., Iwasaki, Y., Maki, N., Mizusawa, H., and Akari, H. (2007). Efficient regulation of viral replication by siRNA in a non-human primate surrogate model for hepatitis C. *Biochem. Biophys. Res. Commun.* 361, 294–300.

Conflict of Interest Statement: The authors declare that the research was conducted in the absence of any commercial or financial relationships that could be construed as a potential conflict of interest.

Received: 21 October 2011; paper pending published: 31 October 2011; accepted: 15 November 2011; published online: 07 December 2011.

Citation: Iwasaki Y, Mori K-i, Ishii K, Maki N, Iijima S, Yoshida T, Okabayashi S, Katakai Y, Lee Y-J, Saito A, Fukai H, Kimura N, Ageyama N, Yoshizaki S, Suzuki T, Yasutomi Y, Miyamura T, Kannagi M and Akari H (2011) Long-term persistent GBV-B infection and development of a chronic and progressive hepatitis C-like disease in marmosets. Front. Microbio. 2:240. doi: 10.3389/fmicb.2011.00240

This article was submitted to Frontiers in Virology, a specialty of Frontiers in Microbiology.

APPENDIX

MATERIALS AND METHODS

Liver samples obtained by necropsy from the GBV-B-infected marmosets were histopathologically analyzed as described in Section "Materials and Methods." Elastica–van Gieson staining was performed to evaluate fibrosis according to a standard laboratory protocol. To detect CD3 and CD20 antigens, liver samples were fixed in 10% neutral buffered formalin and embedded in paraffin wax. Sections were deparaffinized by pretreatment with 0.5% periodic acid and then subjected to antigen retrieval with citric acid buffer and heating in an autoclave for 10 min at 121°C. Sections were then incubated free floating in the monoclonal antibody solution for CD20 (DAKO) and CD3 (DAKO) overnight at 4°C. Following brief washes with buffer, the sections were sequentially incubated with biotinylated goat anti-mouse IgG (1:400), followed by streptavidin–biotin–horseradish peroxidase complex (sABC kit; DAKO, Denmark). Immunoreactive elements were visualized by treating the sections with 3,3′-diaminobenzidine tetroxide (Dojin Kagaku, Japan). The sections were then counterstained with hematoxylin.

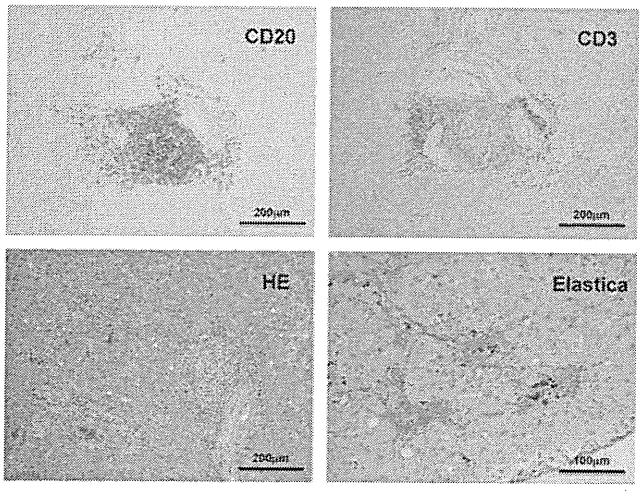

FIGURE A1 | Histopathological and immunohistochemical analyses of the liver from Cj05-004 at week 229 p.i.

UNC93B1 Physically Associates with Human TLR8 and Regulates TLR8-Mediated Signaling

Hiroki Itoh[9], Megumi Tatematsu[9], Ayako Watanabe[9¤], Katsunori Iwano, Kenji Funami, Tsukasa Seya, Misako Matsumoto*

Department of Microbiology and Immunology, Hokkaido University Graduate School of Medicine, Sapporo, Japan

Abstract

Toll-like receptors (TLRs) 3, 7, 8, and 9 are localized to intracellular compartments where they encounter foreign or self nucleic acids and activate innate and adaptive immune responses. The endoplasmic reticulum (ER)-resident membrane protein, UNC93B1, is essential for intracellular trafficking and endolysosomal targeting of TLR7 and TLR9. TLR8 is phylogenetically and structurally related to TLR7 and TLR9, but little is known about its localization or function. In this study, we demonstrate that TLR8 localized to the early endosome and the ER but not to the late endosome or lysosome in human monocytes and HeLa transfectants. UNC93B1 physically associated with human TLR8, similar to TLRs 3, 7, and 9, and played a critical role in TLR8-mediated signaling. Localization analyses of TLR8 tail-truncated mutants revealed that the transmembrane domain and the Toll/interleukin-1 receptor domain were required for proper targeting of TLR8 to the early endosome. Hence, although UNC93B1 participates in intracellular trafficking and signaling for all nucleotide-sensing TLRs, the mode of regulation of TLR localization differs for each TLR.

Citation: Itoh H, Tatematsu M, Watanabe A, Iwano K, Funami K, et al. (2011) UNC93B1 Physically Associates with Human TLR8 and Regulates TLR8-Mediated Signaling. PLoS ONE 6(12): e28500. doi:10.1371/journal.pone.0028500

Editor: Nick Gay, University of Cambridge, United Kingdom

Received August 3, 2011; **Accepted** November 9, 2011; **Published** December 2, 2011

Funding: This work was supported in part by Grants-in-Aid from the Ministry of Education, Science, and Culture, the Ministry of Health, Labor, and Welfare of Japan, and by the Akiyama Life Science Foundation. The funders had no role in study design, data collection and analysis, decision to publish, or preparation of the manuscript.

Competing Interests: The authors have declared that no competing interests exist.

* E-mail: matumoto@pop.med.hokudai.ac.jp

9 These authors contributed equally to this work.

¤ Current address: Department of Cancer Biology, The Institute of Medical Science, The University of Tokyo, Tokyo, Japan

Introduction

The innate immune system discriminates self from non-self by expressing germ-line encoded receptors that recognize pathogen- or damage-associated molecular patterns [1-3]. The Toll-like receptor (TLR) family of type I transmembrane proteins were the first group of pattern recognition receptors to be identified [4]. Within this family, TLRs 3, 7, 8, and 9 recognize microbial nucleic acids and induce cytokine production, including type I interferon (IFN), and dendritic cell (DC) maturation [2]. In humans, TLR7 and TLR9 are selectively expressed in B cells and plasmacytoid DCs, while TLR3 and TLR8 are expressed in myeloid DCs [5–8].

TLR8 is phylogenetically and structurally related to TLR7 [9,10]; they both recognize ssRNA and an imidazoquinoline compound [11–13]. In mice, TLR8 appears to be nonfunctional in most tissues and cells, except for the brain [14,15]. Human TLR8 is expressed in myeloid cells, such as monocytes, macrophages, and myeloid DCs, and also, in regulatory T cells [6,16,17]. Upon stimulation with synthetic ligands, human TLR8 activates NF-κB via the adaptor protein MyD88, which leads to the induction of proinflammatory cytokines but, not type I IFN [13]. In contrast, human/mouse TLR7 strongly induces type I IFN production in response to ssRNA and an imidazoquinoline compound. The differential expression and cytokine profiles of human TLR8 compared with those of human/mouse TLR7 suggest that human TLR8 plays a distinct role in the anti-viral immune response.

Notably, these nucleotide-sensing TLRs are localized to intracellular compartments. Human TLR3 localizes to the early endosome where it recognizes exogenous dsRNA and generates signals via Toll/interleukin-1 receptor (TIR)-containing adaptor molecule-1 (TICAM-1), also named TIR domain-containing adaptor-inducing IFN-β [8,18–20]. A linker region between the transmembrane domain and the TIR domain consisting of 26 amino acids determines the subcellular localization of human TLR3 [21]. In contrast, the transmembrane domain is the main determinant for intracellular localization of mouse TLR7 and TLR9 [22,23]. The endoplasmic reticulum (ER)-resident membrane protein, UNC93B1, physically associates with TLR7 and TLR9 and delivers them to endolysosomes [24,25]. After the trafficking of TLR7 and TLR9 from the ER to the endolysosome, their ectodomains are cleaved to generate a functional receptor [26,27]. UNC93B1 also interacts with TLR3 [24], but its role in the intracellular trafficking of TLR3 remains undefined; however, the interaction of UNC93B1 with the TLR3, 7, and 9 transmembrane regions is essential for the signaling function of these TLRs [28,29]. In contrast, there is little information concerning the subcellular localization and trafficking of human TLR8.

In this study, we analyzed the subcellular localization of TLR8 in human monocytes and HeLa transfectants and demonstrated that TLR8 was localized to the early endosome and the ER but not to the late endosome or lysosome. Using a series of TLR8

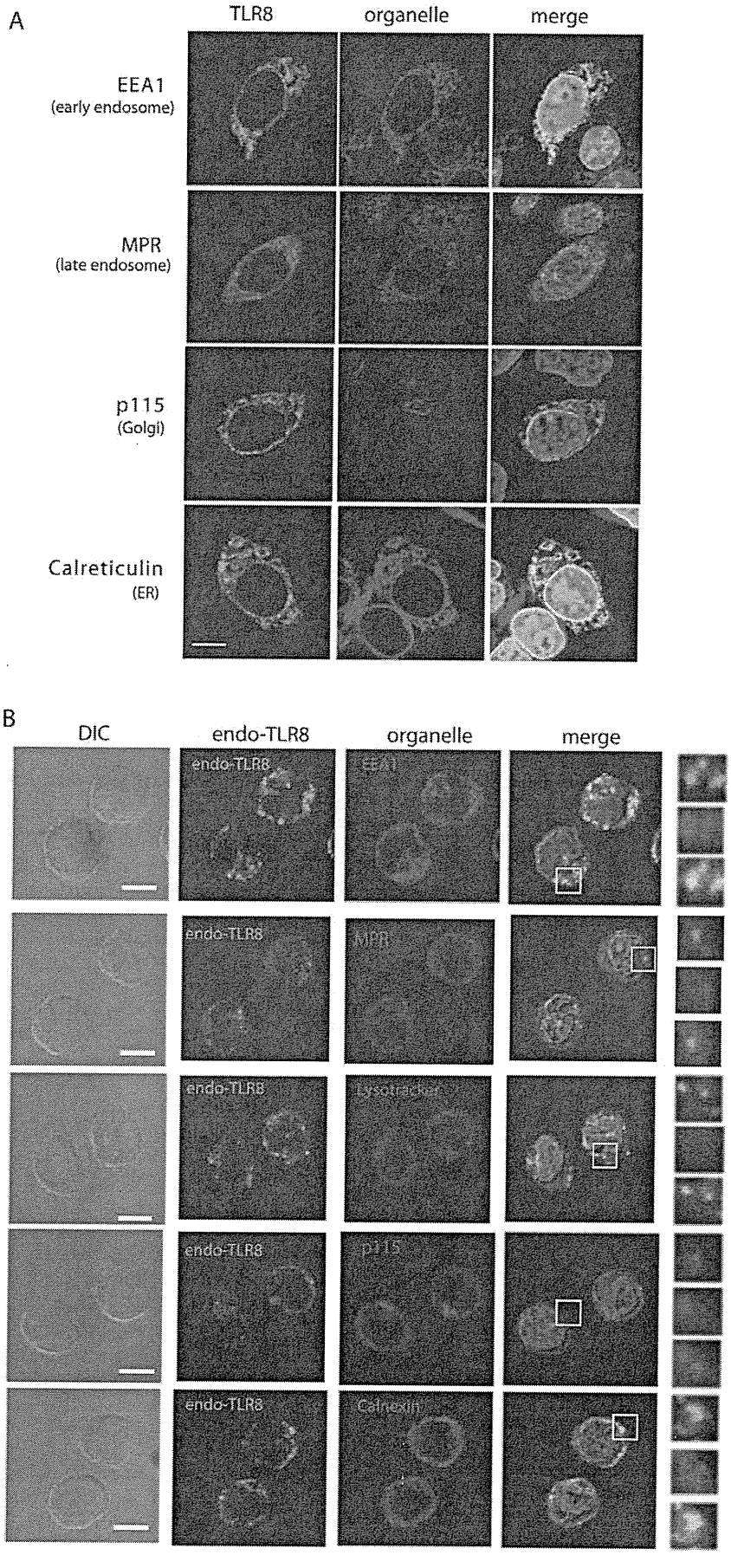
A
TLR8
organelle
merge
EEA1
(early endosome)
MPR
(late endosome)
p115
(Golgi)
Calreticulin
(ER)
B
DIC
endo-TLR8
organelle
merge
endo-TLR8
EEA1
endo-TLR8
MPR
endo-TLR8
Lysotracker
endo-TLR8
p115
endo-TLR8
Calnexin

Figure 1. Subcellular localization of TLR8 in human monocytes and HeLa transfectants. HeLa cells transiently expressing human TLR8 (*A*) and human monocytes (*B*) were incubated with anti-FLAG mAb (*A*) or anti-TLR8 mAb (*B*) followed by an Alexa Fluor 488-conjugated secondary Ab. Organelles were stained with an anti-EEA1 pAb, anti-MPR pAb, anti-p115 pAb, anti-calreticulin pAb, or anti-calnexin pAb followed by an Alexa Fluor 568-conjugated secondary Ab. Representative confocal images are shown. Green, TLR8; red, organelle markers; blue, nuclei stained with DAPI. Scale bar: (*A*) 10 μm; (*B*) 5 μm.
doi:10.1371/journal.pone.0028500.g001

deletion mutants, we demonstrated that both the transmembrane and the TIR domains are required for the intracellular localization of TLR8. Furthermore, we showed that UNC93B1 physically associates with TLR8 and regulates TLR8-mediated signaling.

Results

Human TLR8 localizes to the early endosome and the ER in human monocytes

Intracellular expression of TLR8 was first analyzed using a chimeric receptor composed of the extracellular domain of murine TLR4 fused with the transmembrane and cytoplasmic regions of murine TLR8 [22]. Subsequently, intact human TLR8 was shown to localize intracellularly in transfected cells [30]. However, the site of localization of TLR8 remained unknown. We therefore analyzed the subcellular localization of human TLR8 in HeLa cells transiently expressing FLAG-tagged human TLR8. When examined using confocal microscopy, TLR8-positive compartments colocalized with the early endosome antigen 1 (EEA1) and the ER marker calreticulin (Fig. 1A). Late endosome (MPR), lysosome (LAMP-1), and Golgi (p115) markers did not colocalize with TLR8 (Fig. 1A and data not shown). TLR8 is expressed in human monocytes and induces the cytokine production in response to a synthetic TLR8 ligand [13]; therefore, we next examined the subcellular localization of endogenous TLR8 in human monocytes. TLR8 was localized to the early endosome and the ER but not to the late endosome/lysosome or Golgi (Fig. 1B). Thus, the localization site of TLR8 differed from TLR7 and TLR9, both of which reside in the endolysosome and the ER.

The TIR domain is required for endosomal localization of human TLR8

To determine which region is responsible for the intracellular localization and trafficking of human TLR8, we constructed tail-truncated mutants (Fig. 2A). These included a mutant lacking the TIR domain but retaining the proximal 31 amino acids (delTIR, 1–896 a.a.), one that lacked the cytoplasmic tail (delCYT, 1–866 a.a.), and a mutant lacking the transmembrane domain and the cytoplasmic tail, which anchors the receptor to the membrane via glycosylphosphatidylinositol (GPI) (GPI-TLR8, 45–843 a.a.) (Fig. 2A). When transiently expressed in HEK293FT cells, these mutant proteins were expressed with the expected molecular weight (Fig. 2B). Immunofluorescence staining of HeLa transfectants with anti-FLAG mAb showed that both delTIR and delCYT were displayed on the cell surface (Fig. 2C), while GPI-TLR8 resided only in the ER (Fig. 2C). The lack of expression of GPI-TLR8 on the cell surface was confirmed by flow cytometric analysis with an anti-FLAG mAb (Fig. S1). These results suggest that both transmembrane and the TIR domains are required for proper targeting of human TLR8 to the early endosome.

UNC93B1 physically associates with human TLR8

The ER membrane protein UNC93B1 interacts with TLR3, TLR7, and TLR9 in the ER through the transmembrane domain, and is critical for signaling by these TLRs. Imaging analyses revealed that UNC93B1 regulates intracellular trafficking and endolysosomal targeting of TLR7 and TLR9 [25]. However, its participation in TLR8 localization and signaling remains unknown. To determine the role of UNC93B1 in TLR8 function, we constructed an additional two TLR4/8 chimeric receptors and examined physical interaction between human UNC93B1 and wild-type TLR8, TLR4/8 chimeric receptors, or tail-truncated mutants using co-immunoprecipitation analysis. Chimera TLR4ecto/8 comprised the extracellular domain of TLR4 and the transmembrane and cytoplasmic regions of TLR8, while chimera TLR4/8TIR was composed of the extracellular, transmembrane, and linker regions of TLR4 and the TIR domain of TLR8 (Fig. 3A). As shown in Figure 3B, wild-type TLR8 protein co-immunoprecipitated with UNC93B1 protein in HEK293FT cell lysates, similar to the TLR3 protein. In addition, the TLR4ecto/8 chimeric protein, but not TLR4 and TLR4/8TIR proteins, physically associated with UNC93B1, indicates that the transmembrane region of TLR8 is required for interaction with UNC93B1 (Fig. 3B). Consistent with these results, the TLR8 mutant delCYT associated with UNC93B1, while GPI-TLR8 failed to interact with UNC93B1 (Fig. 3C).

UNC93B1 colocalizes with surface-expressed TLR8 mutants

Since delTIR and delCYT appeared on the cell surface (Fig. 2C), we next examined whether UNC93B1 translocates from the ER to the plasma membrane when these mutants were forcibly expressed in HeLa cells. Interestingly, confocal imaging analysis clearly demonstrated that endogenous UNC93B1 was colocalized with delTIR and delCYT at the plasma membrane, whereas wild-type TLR8 colocalized with UNC93B1 intracellularly (Fig. 4A).

Notably, delTIR and delCYT mutants performed as a dominant-negative against wild-type TLR8. As illustrated in Figure 4B, TLR8-mediated NF-κB activation induced with the TLR8 ligand, CL075 (a thiazoloquinolone derivative), was inhibited by the expression of either delTIR (Fig. 4B, upper graph) or delCYT (Fig. 4B, middle graph) in a dose-dependent manner. In contrast, the expression of GPI-TLR8 did not affect CL075-induced NF-κB activation mediated by wild-type TLR8 (Fig. 4B, lower graph). Thus, the delTIR and delCYT mutants appeared to interfere with the exit of wild-type TLR8 from the ER. Indeed, there was minimal overlay of wild-type TLR8 with EEA1 when co-expressed with these mutants (Fig. S2).

UNC93B1 is essential for TLR8-mediated signaling

Next, we investigated whether UNC93B1 was involved in TLR8-mediated signaling. CL075-induced TLR8-mediated NF-κB activation was greatly increased by the co-expression of UNC93B1 (Fig. 5A). Inversely, knockdown of endogenous UNC93B1 in HEK293 cells downregulated CL075-induced TLR8-mediated NF-κB activation (Fig. 5B). Thus, UNC93B1 is indispensable for TLR8 signaling.

Given that signaling via TLRs 3, 7, and 9 was disrupted in 3d mice, which expresses a UNC93B1 missense mutant (H412R) incapable of TLR binding [29], we constructed a human UNC93B1 mutant, hUNC93B1(H412R), and examined its ability

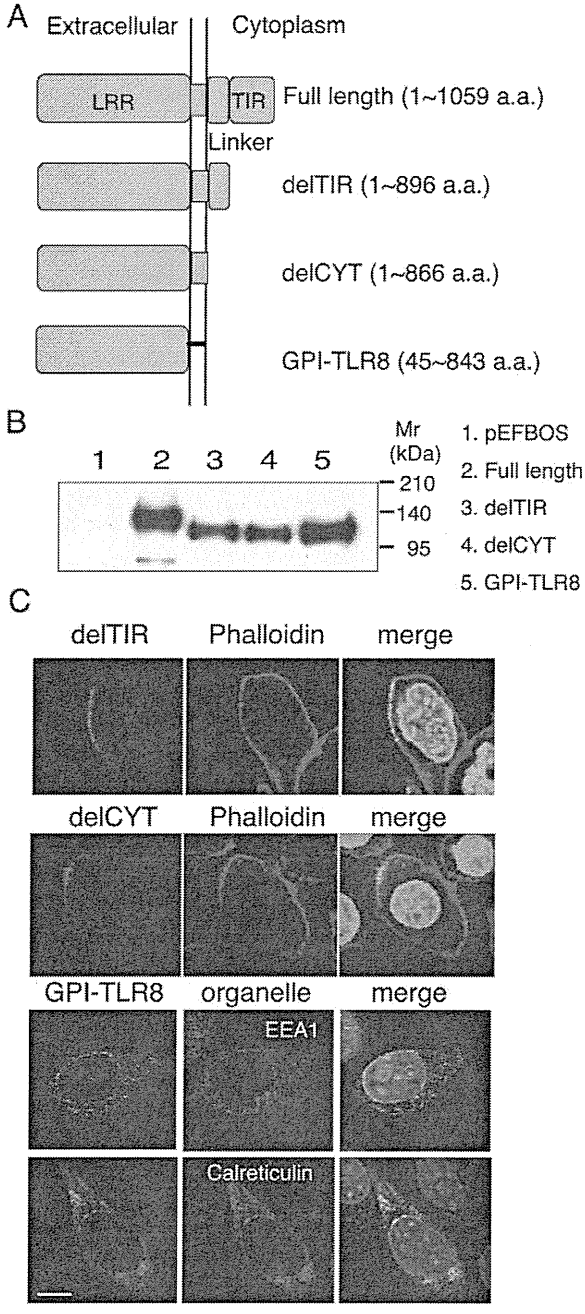

Figure 2. Defining the TLR domain responsible for localization. *A*, Schematic diagram of the tail-deletion constructs of hTLR8. *B*, Expression of the TLR tail-deletion constructs in HEK293FT cells. Wild-type and mutant proteins transiently expressed in HEK293FT cells were immunoprecipitated with anti-FLAG mAb, resolved using SDS-PAGE, and detected using immunoblotting with anti-FLAG mAb. Molecular weight markers are shown on the right. *C*, Immunofluorescence images of the TLR8 deletion constructs in transfected HeLa cells. The upper and middle panels show cells stained with delTIR and delCYT together with phalloidin, which labels the plasma membrane. The lower two panels show cells stained with GPI-TLR8 together with EEA1 or calreticulin. Green, TLR8 mutants; red, organelles; blue, nuclei stained with DAPI; bar, 10 μm.
doi:10.1371/journal.pone.0028500.g002

to bind to TLR8 and mediate signaling. hUNC93B1(H412R) failed to interact with human TLR8, similar to human TLR3 (Fig. 6A). Additionally, forced expression of hUNC93B1(H412R) did not augment CL075-induced TLR8-mediated NF-κB activation (Fig. 6B), suggesting that association of human UNC93B1 with TLR8 through His412 is required for TLR8-mediated signaling as was observed with mouse UNC93B1.

Discussion

Nucleotide-sensing TLRs are divided into two groups based on their distribution profiles in DCs. In humans, TLR3 and TLR8 are expressed in myeloid DCs, while TLR7 and TLR9 are expressed in plasmacytoid DCs [6]. Although TLR8 belongs to the TLR7/8/9 subfamily, the present study demonstrated that TLR8 possesses properties distinct from those of TLR7 and TLR9. First, TLR8, like TLR3, is localized to the early endosome but not in the late endosome/lysosome, where TLR7 and TLR9 reside. Second, although TLR8 requires UNC93B1 to exit from the ER, the TIR domain determines the endosomal targeting of TLR8.

In mouse macrophages and DCs, TLR7 and TLR9 exit the ER and travel to endolysosomes where the ectodomains of both proteins are cleaved to generate functional receptors [26,27]. UNC93B1 controls intracellular trafficking of TLR7 and TLR9 [25,28]. It is obvious that UNC93B1 physically interacts with TLR3, TLR7, and TLR9 in the ER through the transmembrane domain, and is critical for signaling of these TLRs in mice [24,29]. However, prior to this study, it was unclear whether UNC93B1 was involved in TLR8-mediated signaling. We demonstrated the interaction of human UNC93B1 with human TLR8 using a co-immunoprecipitation assay and showed that the up-regulation of TLR8-mediated NF-κB activation in HEK293 cells was induced by the ectopic expression of UNC93B1 (Figs. 3 and 5). The H412R mutation within the transmembrane domain of UNC93B1 disrupted interaction between UNC93B1 and TLR8, and thus failed to increase TLR8-mediated signaling (Fig. 6). Finally, knockdown analysis revealed that UNC93B1 is indispensable for TLR8-mediated signaling (Fig. 5B).

Although UNC93B1 has been shown to deliver TLR7 and TLR9 to endolysosomes where the receptors are cleaved by proteases, this is not the case for TLR8 or TLR3. Gibbard et al. showed that the intact ectodomain of human TLR8 is necessary for dimerization of the receptor and induction of NF-κB activation in response to a synthetic ligand, CL075, in monocytes and HEK293 cells [30]. Hence, TLR8 seems to differ from TLR7 and TLR9 in its mode of ligand recognition. Interestingly, confocal analysis of TLR8 tail-truncated mutants demonstrated that endogenous UNC93B1 moved from the ER to the plasma membrane with the TLR8 mutants. In wild-type TLR8, the TIR domain controls the targeting of TLR8 to the early endosome, although UNC93B1 is required for TLR8 exit from the ER.

The nucleotide-sensing TLRs use different regulatory elements for intracellular localization. In the case of mouse TLR7 and TLR9, the transmembrane domain determines the intracellular localization of the receptor. However, Leifer et al. reported that the cytoplasmic tail of human TLR9 controls intracellular localization [31]. A 14-amino acid region in the hTLR9-TIR domain targets the Tac (human CD25)-TLR9 chimeric receptor to early endosomes. Additionally, a recent report demonstrated that bovine TLR8 localized to the ER, and that multiple regions, including ectodomain, transmembrane, linker, and TIR regions of bovine TLR8, are involved in determining the intracellular localization [32]. Thus, there may be species-specific regulatory mechanisms of intracellular localization of TLRs.

The mechanism by which TLR8 is retained in the early endosome is currently unknown. It is likely that an unidentified

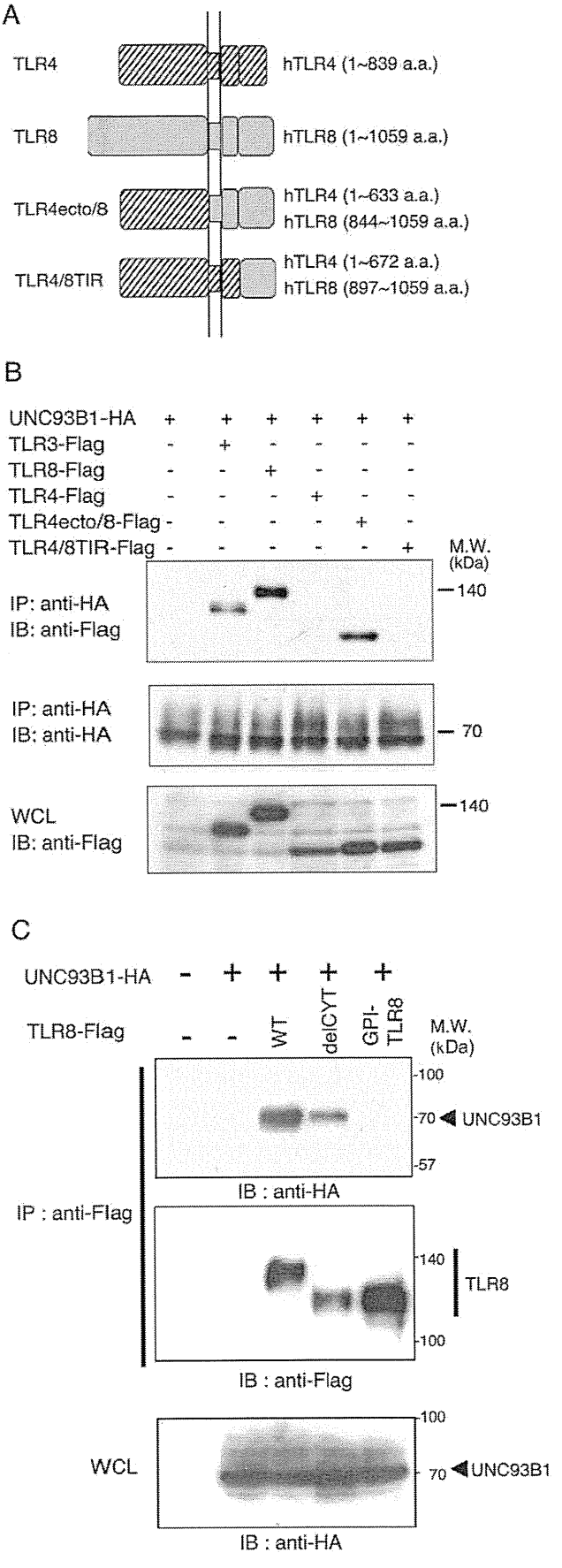

Figure 3. UNC93B1 physically associates with TLR8 through the transmembrane domain in HEK293FT cells. *A*, Schematic diagram of the TLR4/8 chimeric receptor constructs. *B*, *C*, HEK293FT cells were transfected with the corresponding vectors for expression of the indicated proteins. Twenty-four hours after transfection, cells were lysed in lysis buffer. The lysates were immunoprecipitated (IP) with anti-HA pAb (*B*) or anti-FLAG pAb (*C*), resolved using SDS-PAGE, and detected using immunoblotting (IB) with anti-FLAG M2 mAb or anti-HA mAb. Whole cell lysates (WCL) were subjected to immunoblotting with anti-FLAG mAb (*B*) or anti-HA mAb (*C*) to detect protein expression. Molecular weight markers are shown on the right.
doi:10.1371/journal.pone.0028500.g003

molecule interacts with the TIR domain of TLR8 and facilitates its trafficking to the early endosomes. As the BB loop in the TLR-TIR domain is critical for interaction with adaptor proteins, another region of the TLR8-TIR domain may participate in the association with the protein(s) regulating the receptor trafficking and intracellular localization of TLR8.

In humans, TLR7 and TLR8 recognize sequence-specific ssRNA and imidazoquinoline compounds in distinct cells and organelles, resulting in the induction of different immune responses via the same adaptor protein, MyD88. TLR7 ligands induce IFN-α production by plasmacytoid DCs, while TLR8 ligands induce proinflammatory cytokine production (e.g., TNF-α and IL-6) by myeloid DCs and monocytes [13]. This implies that TLR7 and TLR8 play distinct roles in the anti-viral immune response. Myeloid DCs express the viral RNA sensors, TLR3 and TLR8, on the endosomal membrane where they recognize virus-derived dsRNA and ssRNA, respectively. Activation of TLR3 by dsRNA results in the production of T helper 1 cytokines, such as IFN-α/β and interleukin (IL)-12p70, as well as DC maturation leading to the activation of cytotoxic T lymphocytes and natural killer (NK) cells [33]. TLR3 activation also induces TICAM-1-dependent gene expression in myeloid DCs, which mediates DC–NK reciprocal activation through cell–cell contact independently of type I IFN and IL-12 [34], whereas the key role of TLR8-mediated myeloid DC activation remains poorly understood. Detailed analyses of TLR8-mediated signaling in different cell types may give us new insight into the function of TLR8 in the anti-viral response.

Materials and Methods

Cell culture and reagents

HEK293 cells were maintained in Dulbecco's Modified Eagle's medium low glucose (Invitrogen) supplemented with 10% heat-inactivated FCS (BioSource Intl., Inc.) and antibiotics. HEK293FT cells were maintained in Dulbecco's Modified Eagle's medium high glucose supplemented with 0.1 mM NEAA, 10% heat-inactivated FCS and antibiotics. HeLa cells were maintained in Eagle's MEM (Nissui, Tokyo, Japan) supplemented with 1% L-glutamine and 10% heat-inactivated FCS. Human monocytes were isolated from peripheral blood mononuclear cells obtained from healthy individuals with a magnetic cell sorting system using anti-CD14-coated microbeads (Miltenyi Biotec, Gladbach, Germany). Anti-FLAG M2 monoclonal antibody (mAb), anti-HA polyclonal Ab (pAb), 4′,6-diamidine-2′-phenylindole dihydrochloride (DAPI), TRITC-labeled anti-phalloidin Ab, and saponin were purchased from Sigma-Aldrich. In addition, the following antibodies were used in this study: Alexa Fluor-conjugated secondary antibodies (Invitrogen), anti-HA mAb (Covance), anti-early endosome antigen 1 (EEA1) pAb (Affinity Bioreagents), anti-calnexin pAb and anti-calreticulin pAb (Stressgen, Victoria, Canada), anti-p115 pAb (Calbiochem, Darmstadt, Germany),

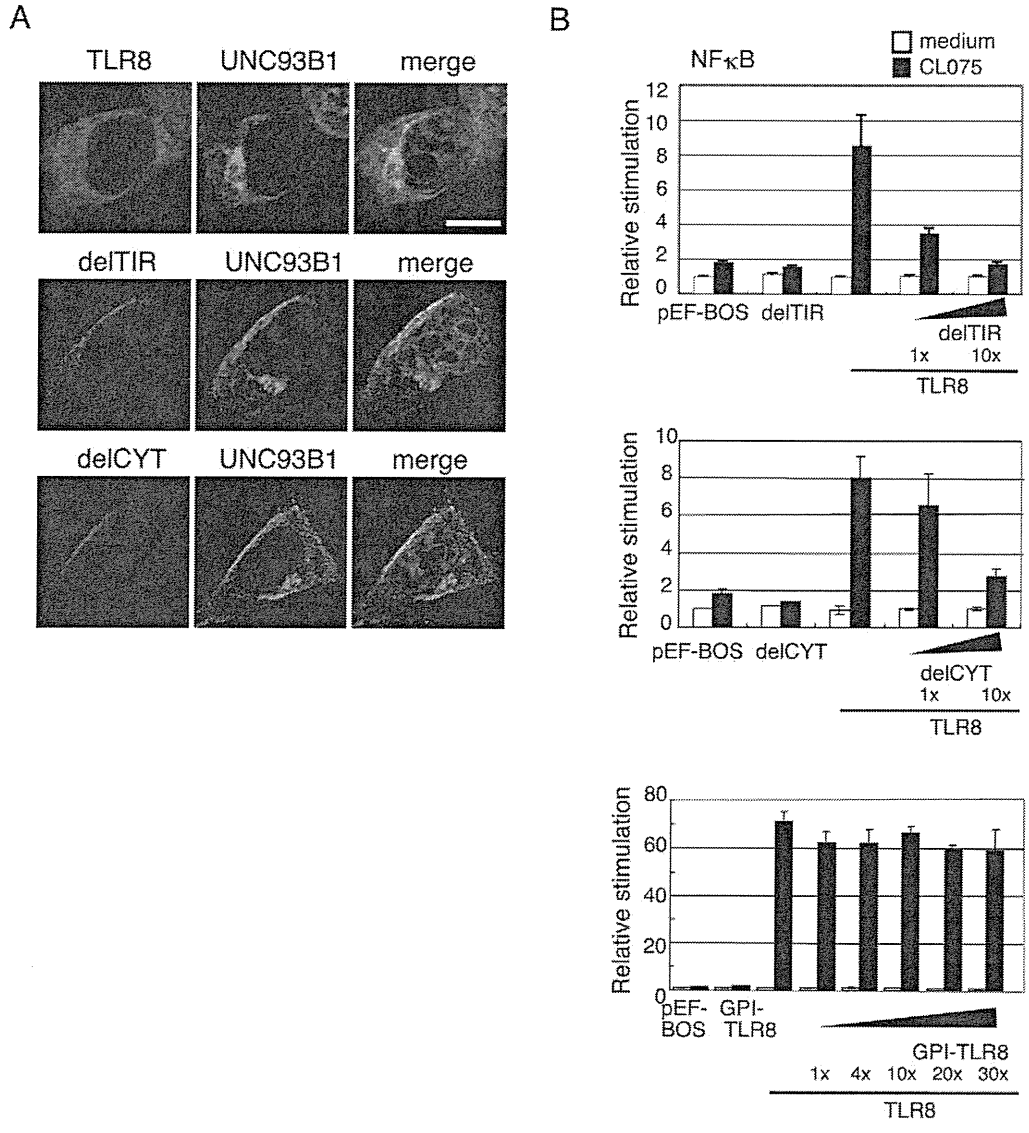

Figure 4. UNC93B1 colocalizes with surface-expressed TLR8 mutants. *A*, HeLa cells transiently expressing wild-type TLR8, delCYT, or delTIR were incubated with anti-FLAG mAb and anti-human UNC93B1 pAb followed by an Alexa Fluor 568-conjugated anti-mouse IgG and Alexa Fluor 488-conjugated anti-rabbit IgG. Representative confocal images are shown. Green, endogenous UNC93B1; red, TLR8; blue, nuclei stained with DAPI. Scale bar:10 μm. *B*, Surface-expressed TLR8 mutant proteins inhibited CL075-induced TLR8-mediated NF-κB activation. Luciferase activity of HEK293 cells transfected with the ELAM-promoter-luciferase reporter and expression plasmid for wild-type TLR8 together with increasing amounts of plasmid expressing delTIR (upper graph), delCYT (middle graph), or GPI-TLR8 (lower graph). Twenty-four hours after transfection, the cells were stimulated with 2.5 μg/mL of CL075 or left untreated. After 24 hours, the luciferase reporter activities were measured and expressed as the fold induction relative to the activity of unstimulated cells. Representative data from a minimum of three separate experiments are shown (mean and s.d. of triplicate assays).
doi:10.1371/journal.pone.0028500.g004

anti-LAMP-1 mAb (Biolegend), anti-MPR pAb (Abcam, Cambridge, UK), anti-human TLR8 mAb (Dendritics, LYON, France) and anti-human UNC93B1 pAb (ProSci Inc., Poway, CA). Lysotracker was from Invitrogen. CL075 was from InvivoGen.

Plasmids

Complementary DNAs for human TLR3 and TLR8 were cloned in our laboratory by RT-PCR from the mRNA of monocyte-derived immature DCs and were ligated into the cloning site of the expression vector, pEF-BOS, which was provided by Dr. S. Nagata (Kyoto University). The FLAG-tag or HA-tag was inserted into the C-terminal of pEF-BOS expression vectors for hTLR3 or hTLR8. The truncated TLR8 mutants, delTIR (1-896 a.a.) and delCYT (1-866 a.a.) were generated by PCR with Pfu Turbo DNA polymerase (STRATAGENE) using specific primers (forward primer; 5′-GACTACAAAGACGATGACGACAAGTAAGCG-3′, reverse primer for delTIR; 5′-GAAAGTTTGCGATGTGGAAAGAGACCTGTA-3′, reverse primer for delCYT; 5′-AGCCAGGGCAGCCAACATAACCATGGTGGT-3′) as described [21]. GPI-hTLR8 was constructed in the pEF-BOS expression vector by ligation of PCR products corresponding to the TLR8 ectodomain (45-843 a.a.) sequentially attached with the preprotrypsin signal sequence, HAT, and Flag at the N-terminus, and the GPI-attachment sequence from CD55 at

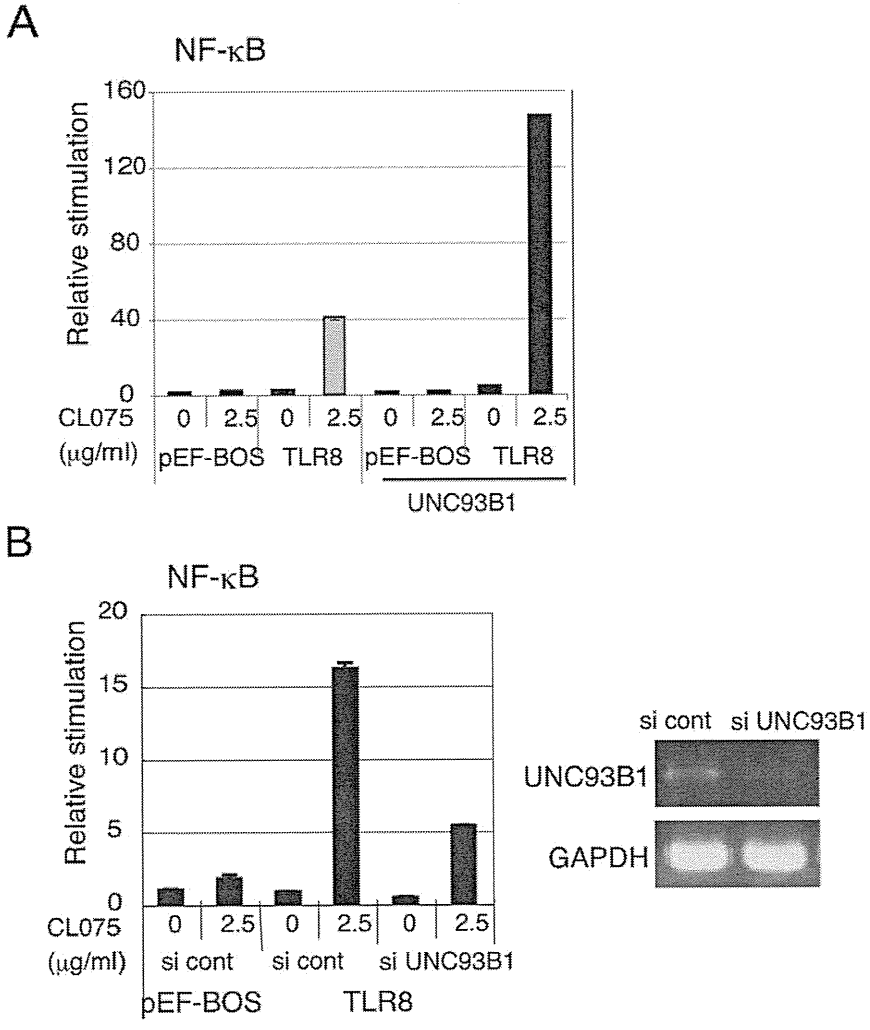

Figure 5. UNC93B1 is indispensable for TLR8-mediated signaling. *A*, Upregulation of TLR8-mediated NF-κB activation by co-expression with UNC93B. HEK293 cells were transfected with the indicated plasmid together with the ELAM reporter plasmid. Twenty-four hours after transfection, the cells were stimulated with CL075 or left untreated. After 6 hours, the luciferase reporter activities were measured and expressed as the fold induction relative to the activity of unstimulated cells. Representative data from three separate experiments are shown. *B*, TLR8-mediated NF-κB activation is downregulated by knockdown of UNC93B1. UNC93B1 siRNA or negative control siRNA was transfected into HEK293 cells together with the reporter plasmids and TLR8 expression plasmid. Forty-eight hours after transfection, cells were stimulated with CL075 for 6 hours and the luciferase reporter activities were measured. Data are representative of three independent experiments (mean and s.d. of triplicate assays). The expression of endogenous UNC93B1 and GAPDH mRNAs were examined using RT-PCR 48 hours after siRNA transfection (right panels).
doi:10.1371/journal.pone.0028500.g005

the C-terminus. The TLR4/TLR8 chimeric receptor, TLR4ecto/8, was constructed in the expression vector pEF-BOS by ligation of PCR products corresponding to amino acids 1-633 of human TLR4 ectodomain and amino acids 844-1059 of human TLR8. Another TLR4/TLR8 chimeric receptor, TLR4/8TIR, was constructed by the ligation of PCR products corresponding to amino acids 1-672 of human TLR4 (ectodomain, TM, and linker region) and amino acids 897-1059 of the human TLR8 TIR domain. Both constructs were FLAG tagged at the C-terminus. A plasmid for human UNC93B1 (pMD2/UNC93B1) and the expression plasmid for TLR4 (pEF-BOS/TLR4) were provided by Dr. K. Miyake (The University of Tokyo). The HA-tag was inserted into the C-terminal of the pEF-BOS expression vector for human UNC93B1. The human UNC93B1 mutant, hUNC93B1(H412R), in which the arginine residue at position 412 was substituted for a histidine residue, was made by site-directed mutagenesis.

Confocal microscopy

HeLa cells (1.0×10^5 cells/well) were plated onto micro cover glasses (Matsunami, Tokyo, Japan) in a 24-well plate. The following day, cells were transfected with the indicated plasmids using Fugene HD (Roche Diagnostics) or Lipofectamine 2000 (Invitrogen). Twenty-four hours after transfection, cells were fixed with 3% formalin for 30 min and permeabilized with PBS containing 0.5% saponin and 1% BSA for 30 min or fixed with 4% paraformaldehyde for 30 min and permeabilized with PBS containing 0.2% Triton X-100 and 1% BSA for 15 min (for staining of endogenous UNC93B1). In the case of monocytes, cells were fixed with 4% paraformaldehyde for 15 min. For the staining of late endosome, cells were permeabilized with PBS containing 100 μg/ml of digitonin and 1% BSA for 30 minutes. Fixed cells were blocked in PBS containing 1% BSA, and were then labeled with the indicated primary Abs (2~10 μg/ml) for 60 min at room temperature. Alexa-conjugated secondary Abs (1:400) were used

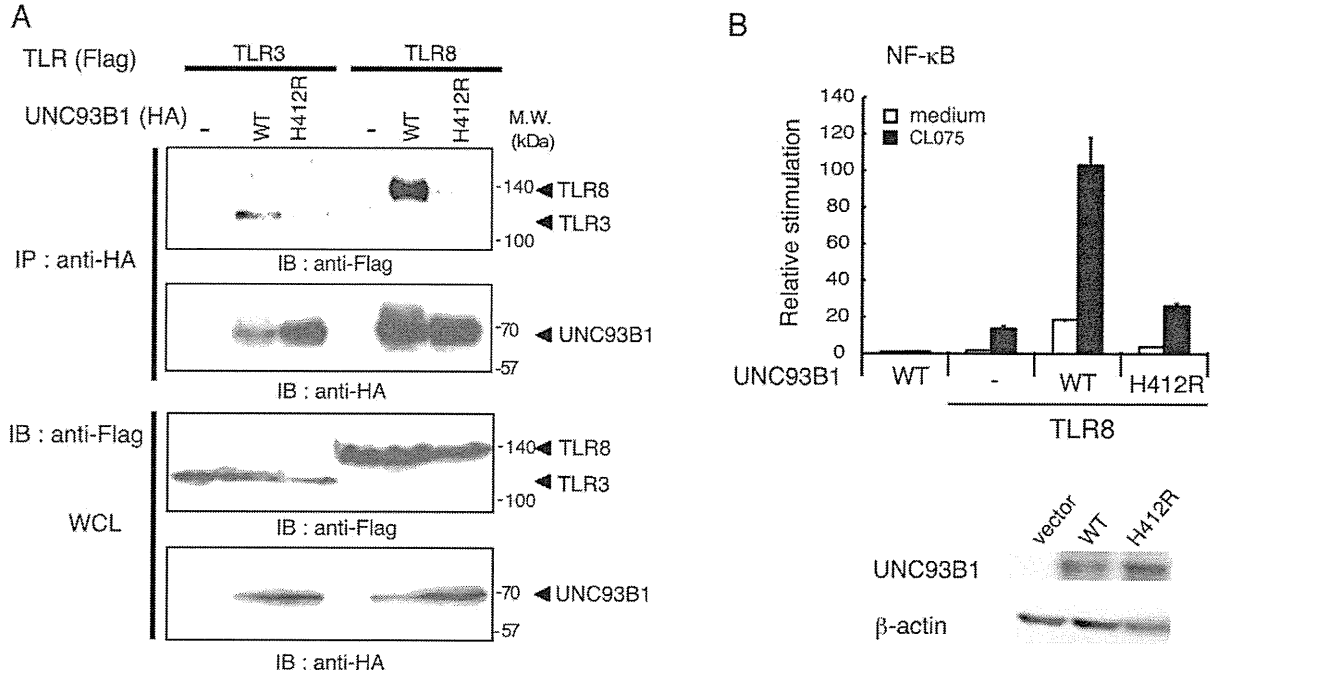

Figure 6. His412 is essential for the interaction of UNC93B1 with TLR8 and TLR8-mediated signaling. *A*, HEK293FT cells were transfected with the corresponding vectors for expression of the indicated proteins. The cell lysates were immunoprecipitated (IP) with anti-HA pAb, resolved by SDS-PAGE and detected by immunoblotting (IB) with anti-FLAG M2 or anti-HA mAb. Whole cell lysates (WCL) were subjected to immunoblotting with anti-FLAG or anti-HA mAb to detect protein expression. Molecular weight markers are shown on the right. *B*, HEK293 cells were transfected with the indicated plasmid together with the ELAM reporter plasmid. Cells were stimulated with CL075 or left untreated and the luciferase reporter activities were measured. Representative data from three separate experiments are shown. *Lower panels,* protein expression of wild-type and mutant UNC93B1 in HEK293 cells. β-actin blots are shown as loading controls.
doi:10.1371/journal.pone.0028500.g006

to visualize the staining of the primary Abs. After mounting with ProLong Gold with DAPI (Molecular Probes), cells were visualized at a magnification of ×63 with an LSM510 META microscope (Zeiss, Jena, Germany).

Reporter assay

HEK293 cells (5×10^5 cells/well) cultured in 24-well plates were transfected with the indicated plasmid together with the reporter plasmid and an internal control vector, phRL-TK (Promega), using FuGENE HD. The reporter plasmid containing the ELAM-1 promoter was constructed in our laboratory. Twenty-four hours after transfection, cells were stimulated with 2.5 μg/mL CL075. The cells were collected 6 hours after stimulation and then lysed. The *Firefly* and *Renilla* luciferase activities were determined using a dual-luciferase reporter assay kit (Promega). The *Firefly* luciferase activity was normalized with the *Renilla* luciferase activity and was expressed as the fold induction relative to the activity in unstimulated vector-transfected cells. All assays were performed in triplicate.

RNAi

siRNA duplexes (UNC93B1:ID #s37730, negative control: catalog #AM4635) were obtained from Ambion-Applied Biosystems. HEK293 cells cultured in 24-well plates were transfected with 20 pmol of each siRNA together with the expression vector for hTLR8 (40 ng), ELAM reporter plasmid (60 ng), an internal control vector (1.5 ng) and empty vector (400 ng) using Lipofectamin 2000. Forty-eight hours after transfection, cells were washed once and then stimulated with 2.5 μg/ml CL075 for 6 hours. Knockdown of UNC93B1 was confirmed 48 hours after siRNA transfection by RT-PCR using specific primers (UNC93B1: forward primer 5′-GCCCATGATTTATTTCCTGAACCACTACC-3′ and reverse primer, 5′-GTGTGCTGAGTCCAGTCTTGTTCAG-3′, GAPDH: forward primer 5′-GAGTCAACGGATTTGGTCGT-3′ and reverse primer 5′- TTGATTTTGGAGGGATCTCG-3′). Experiments were repeated three times for confirmation of the results.

Immunoprecipitation

HEK293FT cells (2.5×10^5 cells/well) cultured in 12-well plates were transfected with the indicated plasmids using Lipofectamine 2000 (Invitrogen). After 24 hours, cells were washed twice with DPBS. Washed cells were lysed in 1% digitonin lysis buffer (50 mM Tris-HCl (pH 7.4), 150 mM NaCl, 5 mM EDTA, 2 mM PMSF, and a protease inhibitor cocktail) or 1% NP-40 lysis-washing buffer (50 mM Tris-HCl (pH 7.4), 150 mM NaCl, 10 mM EDTA, 1 mM PMSF, and a protease inhibitor cocktail) in Fig. 2. Lysates were clarified by centrifugation, pre-cleared with Protein G-Sepharose (GE Healthcare, Buckinghamshire, UK), and incubated with anti-FLAG mAb or anti-HA pAb. The immunoprecipitates were recovered by incubation with Protein G-Sepharose, washed three times with 0.1% digitonin washing buffer (50 mM Tris-HCl (pH 7.4), 150 mM NaCl, 5 mM EDTA, 1 mM PMSF) or 1% NP-40 lysis-washing buffer and then resuspended in denaturing buffer. Samples were analyzed by SDS-PAGE under reducing conditions followed by immunoblotting with anti-tag Abs.

Supporting Information

Figure S1 Flow cytometric analysis of cell surface expression of GPI-hTLR8 transiently expressed in HeLa cells. HeLa cells were

transfected with the empty vector or the expression plasmid for FLAG-tagged GPI-hTLR8 using Lipofectamine 2000 in 12-well plates. Twenty-four hours after transfection, cells were washed and incubated with anti-FLAG M2 mAb or mouse IgG1 in the presence of human IgG for 30 min at 4° C in FACS buffer (DPBS containing 0.5% BSA and 0.1% sodium azide). Cells were washed twice in FACS buffer and incubated with FITC-labeled secondary antibody (American Qualex) for 30 min at 4° C. For intracellular staining, cells were permeabilized with permeabilizing solution (BD) for 10 min at room temperature, and then stained with anti-FLAG mAb in the presence of 10% goat serum and FITC-labeled secondary Ab. Cells were analyzed using a FACS Calibur (BD). Shaded histogram: control mouse IgG 1 staining; thick line: anti-FLAG mAb staining. Inset values indicate the mean fluorescent intensities specific for the anti-FLAG mAb.
(EPS)

Figure S2 Forced expression of TLR8 mutants affects the endosomal localization of wild-type TLR8. *A*, Confocal images show HeLa cells co-expressing HA-tagged wild-type TLR8 and FLAG-tagged TLR8 mutants. Cells were fixed and stained with anti-FLAG mAb and anti-HA pAb, followed by Alexa568-labeled goat anti-mouse Ab and Alexa488-labeled goat anti-rabbit Ab. TLR8 mutants delCYT and delTIR were anchored on plasma membrane and did not merge with wild-type TLR8. Red, TLR8 mutants; green, wild-type TLR8; blue, nuclei stained with DAPI; bar, 10 μm. *B*, Cells were transfected with FLAG-tagged wild-type TLR8 alone (upper panels), together with FLAG-tagged delCYT (middle panels) or FLAG-tagged delTIR (lower panels), and stained with anti-FLAG mAb and anti-EEA1 pAb, followed by Alexa568-labeled goat anti-mouse Ab and Alexa488-labeled goat anti-rabbit Ab. Wild-type TLR8 was expressed intracellularly and colocalized with EEA1 (upper panels). When delCYT or delTIR was expressed with wild-type TLR8, colocalization between TLR8 and EEA1 was decreased (middle and lower panels). Red, TLR8; green, early endosome marker EEA1; blue, nuclei stained with DAPI; bar, 10 μm.
(EPS)

Acknowledgments

We are grateful to Drs. H. Oshiumi, H. Shime, T. Ebihara, A. Matsuo, H. H. Aly, H. Takaki, and J. Kasamatsu for invaluable discussions. Thanks are also due to Dr. K. Miyake (University of Tokyo, Tokyo) for providing plasmids.

Author Contributions

Conceived and designed the experiments: HI KF TS MM. Performed the experiments: HI MT AW KI. Analyzed the data: MT TS MM. Wrote the paper: MM.

References

1. Medzhitov R, Janeway CA, Jr. (1997) Innate immunity: the virtues of a nonclonal system of recognition. Cell 91: 295–298.
2. Akira S, Uematsu S, Takeuchi O (2006) Pathogen recognition and innate immunity. Cell 124: 783–801.
3. Kono H, Rock KL (2008) How dying cells alert the immune system to danger. Nat Rev Immunol 8: 279–289.
4. Medzhitov R, Preston-Hurlburt P, Janeway CA, Jr. (1997) A human homologue of the Drosophila Toll protein signals activation of adaptive immunity. Nature 388: 394–397.
5. Muzio M, Bosisio D, Polentarutti N, D'amico G, Stoppacciaro A, et al. (2000) Differential expression and regulation of toll-like receptors (TLR) in human leukocytes: selective expression of TLR3 in dendritic cells. J Immunol 164: 5998–6004.
6. Kadowaki M, Ho S, Antonenko S, de Waal Malefyt R, Kastelein RA, et al. (2001) Subsets of human dendritic cell precursors express different Toll-like receptors and respond to different microbial antigens. J Exp Med 194: 863–870.
7. Hornung V, Rothenfusser S, Britsch S, Krug A, Jahrsdorfer B, et al. (2002) Quantitative expression of Toll-like receptor 1-10 mRNA in cellular subsets of human peripheral blood mononuclear cells and sensitivity to CpG oligodeoxynucleotides. J Immunol 168: 4531–4537.
8. Matsumoto M, Funami K, Tanabe M, Oshiumi H, Shingai M, et al. (2003) Subcellular localization of Toll-like receptor 3 in human dendritic cells. J Immunol 171: 3154–3162.
9. Chuang T-H, Ulevitch RJ (2000) Cloning and characterization of a sub-family of human Toll-like receptors: hTLR7, hTLR8 and hTLR9. Eur Cytokine Netw 11: 372–378.
10. Du X, Poltorak A, Wei Y, Beutler B (2000) Three novel mammalian toll-like receptors: gene structure, expression, and evolution. Eur Cytokine Netw 11: 362–371.
11. Heil F, Hemmi H, Hochrein H, Ampenberger F, Kirschning C, et al. (2004) Species-specific recognition of single-stranded RNA via toll-like receptor 7 and 8. Science 303: 1526–1529.
12. Diebold SS, Kaisho T, Hemmi H, Akira S, Sousa RC (2004) Innate antivial responses by means of TLR7-mediated recognition of single-stranded RNA. Science 303: 1529–1531.
13. Gorden KB, Gorski KS, Gibson SJ, Kedl RM, Kieper WC, et al. (2005) Synthetic TLR agonists reveal functional differences between human TLR7 and TLR8. J Immunol 174: 1259–1268.
14. Jurk M, Heil F, Vollmer J, Schetter C, Krieg AM, et al. (2002) Human TLR7 or TLR8 independently confer responsiveness to the antiviral compound R-848. Nat Immunol 3: 499.
15. Ma Y, Li J, Chiu I, Wang Y, Sloane JA, et al. (2006) Toll-like receptor 8 functions as a negative regulator of neurite outgrowth and inducer of neuronal apoptosis. J Cell Biol 28: 209–215.
16. Peng G, Guo Z, Kiniwa Y, Voo KS, Peng W Fu, et al. (2005) Toll-like receptor 8-mediated reversal of CD4+ regulatory T cell function. Science 309: 1380–1384.
17. Jongbloed SL, Kassianos AJ, McDonald KJ, Clark GJ, Ju X, et al. (2010) Human CD141+ (BDCA-3+) dendritic cells (DCs) represent a unique myeloid DC subset that cross-presents necrotic cell antigens. J Exp Med 207: 1247–1260.
18. Oshiumi H, Matsumoto M, Funami K, Akazawa T, Seya T (2003) TICAM-1, an adaptor molecule that participates in Toll-like receptor 3-mediated interferon-beta induction. Nat Immunol 4: 161–167.
19. Yamamoto M, Sato S, Hemmi H, Hoshino K, Kaisho T, et al. (2003) Role of adaptor TRIF in the MyD88-independent Toll-like receptor signaling pathway. Science 301: 640–643.
20. Funami K, Sasai M, Ohba Y, Oshiumi H, Seya T, et al. (2007) Spatiotemporal mobilization of Toll/IL-1 receptor domain-containing adaptor molecule-1 in response to dsRNA. J Immunol 179: 6867–6872.
21. Funami K, Matsumoto M, Oshiumi H, Akazawa T, Yamamoto A, et al. (2004) The cytoplasmic 'linker region' in Toll-like receptor 3 controls localization and signaling. Int Immunol 16: 1143–1154.
22. Nishiya T, DeFranco AL (2004) Ligand-regulated chimeric receptor approach reveals distinctive subcellular localization and signaling properties of the Toll-like receptors. J Biol Chem 279: 19008–19017.
23. Barton GM, Kagan JC, Medzhitov R (2006) Intracellular localization of Toll-like receptor 9 prevents recognition of self DNA but facilitates access to viral DNA. Nat Immunol 7: 49–56.
24. Brinkmann MM, Spooner E, Hoebe K, Beutler B, Ploegh HL, et al. (2007) The interaction between the ER membrane protein UNC93B and TLR3, 7, and 9 is crucial for TLR signaling. J Cell Biol 177: 265–275.
25. Kim Y-M, Brinkmann MM, Paquet M-E, Ploegh HL (2008) UNC93B1 delivers nucleotide-sensing toll-like receptors to endolysosomes. Nature 452: 234–238.
26. Ewald SE, Lee BL, Lau L, Wickliffe KE, Shi G-P, et al. (2008) The ectodomain of Toll-like receptor 9 is cleaved to generate a functional receptor. Nature 456: 658–662.
27. Park B, Brinkmann MM, Spooner E, Lee CC, Kim YM, et al. (2008) Proteolytic cleavage in an endolysosomal compartment is required for activation of Toll-like receptor 9. Nat Immunol 9: 1407–141.
28. Fukui R, Saitoh S, Matsumoto F, Kozuka-Hara H, Oyama M, et al. (2009) Unc93B1 biases Toll-like receptor responses to nucleic acid in dendritic cells toward DNA- but against RNA-sensing. J Exp Med 206: 1339–1350.
29. Tabeta K, Hoebe K, Janssen EM, Du X, Georgel P, et al. (2006) The Unc93B1 mutation 3d disrupts exogeneous antigen presentation and signaling via Toll-like receptors 3, 7 and 9. Nat Immunol 7: 146–164.
30. Gibbard RJ, Morley, PJ, Gay NJ (2006) Conserved features in the extracellular domain of human Toll-like receptor 8 are essential for pH-dependent signaling. J Biol Chem 281: 27503–27511.
31. Leifer CA, Brooks JC, Hoelzer K, Lopez J, Kennedy MN, et al. (2006) Cytoplasmic Targeting motifs control localization of Toll-like receptor 9. J Biol Chem 281: 35585–35592.
32. Zhua J, van Drunen Littel-van den Hurka S, Brownliea R, Babiuka LA, Pottera A, et al. (2009) Multiple molecular regions confer intracellular localization of bovine Toll-like receptor 8. Molec Immunol 46: 884–892.

33. Matsumoto M, Seya T (2008) TLR3: Interferon induction by double-stranded RNA including poly(I:C). Adv Drug Del Rev 60: 805–812.

34. Ebihara T, Azuma M, Oshiumi H, Kasamatsu J, Iwabuchi K, et al. (2010) Identification of a polyI:C-inducible membrane protein that participates in dendritic cell-mediated natural killer cell activation. J Exp Med 207: 2675–2687.

Herpes simplex encephalitis in children with autosomal recessive and dominant TRIF deficiency

Vanessa Sancho-Shimizu,[1,2] Rebeca Pérez de Diego,[1,2] Lazaro Lorenzo,[1,2] Rabih Halwani,[3] Abdullah Alangari,[3] Elisabeth Israelsson,[4] Sylvie Fabrega,[5] Annabelle Cardon,[1,2] Jerome Maluenda,[1,2] Megumi Tatematsu,[6] Farhad Mahvelati,[7] Melina Herman,[8] Michael Ciancanelli,[8] Yiqi Guo,[8] Zobaida AlSum,[3] Nouf Alkhamis,[3] Abdulkarim S. Al-Makadma,[9] Ata Ghadiri,[10,11] Soraya Boucherit,[1,2] Sabine Plancoulaine,[1,2] Capucine Picard,[1,2,12,13] Flore Rozenberg,[14] Marc Tardieu,[15] Pierre Lebon,[14] Emmanuelle Jouanguy,[1,2,13] Nima Rezaei,[16,17] Tsukasa Seya,[6] Misako Matsumoto,[6] Damien Chaussabel,[4] Anne Puel,[1,2] Shen-Ying Zhang,[1,8] Laurent Abel,[1,2,8] Saleh Al-Muhsen,[3] and Jean-Laurent Casanova[1,2,3,8,12]

[1]Laboratory of Human Genetics of Infectious Diseases, Necker Branch, Institut National de la Santé et de la Recherche Médicale, Necker Medical School, Paris, France. [2]University Paris Descartes, Paris, France. [3]Prince Naif Center for Immunology Research, Department of Pediatrics, College of Medicine, King Saud University, Riyadh, Saudi Arabia. [4]Benaroya Research Institute at Virginia Mason, Seattle, Washington, USA. [5]Viral Vector and Gene Transfer Platform, University Paris Descartes, Institut Fédératif de Recherche Necker Enfants Malades, Paris, France. [6]Department of Microbiology and Immunology, Hokkaido University Graduate School of Medicine, Sapporo, Japan. [7]Child Neurology Department, Mofid Children Hospital, Shahid Beheshti University of Medical Sciences, Tehran, Iran. [8]Laboratory of Human Genetics of Infectious Diseases, Rockefeller Branch, The Rockefeller University, New York, New York, USA. [9]King Fahd Medical City, Riyadh, Saudi Arabia. [10]Department of AIDS and Hepatitis, Pasteur Institute, Tehran, Iran. [11]Department of Immunology, Faculty of Medicine, Ahvaz Jundishapur University of Medical Sciences, Ahvaz, Iran. [12]Pediatric Hematology-Immunology Unit and [13]Study Center of Primary Immunodeficiencies, Necker Hospital, Paris, France. [14]Virology, Cochin Hospital, University Paris Descartes, Paris, France. [15]Pediatric Neurology, Bicêtre Hospital, University Paris Sud, Kremlin-Bicêtre, France. [16]Research Center for Immunodeficiencies, Pediatrics Center of Excellence, Children's Medical Center, and [17]Molecular Immunology Research Center and Department of Immunology, School of Medicine, Tehran University of Medical Sciences, Tehran, Iran.

Herpes simplex encephalitis (HSE) is the most common sporadic viral encephalitis of childhood. Autosomal recessive (AR) UNC-93B and TLR3 deficiencies and autosomal dominant (AD) TLR3 and TRAF3 deficiencies underlie HSE in some children. We report here unrelated HSE children with AR or AD TRIF deficiency. The AR form of the disease was found to be due to a homozygous nonsense mutation that resulted in a complete absence of the TRIF protein. Both the TLR3- and the TRIF-dependent TLR4 signaling pathways were abolished. The AD form of disease was found to be due to a heterozygous missense mutation, resulting in a dysfunctional protein. In this form of the disease, the TLR3 signaling pathway was impaired, whereas the TRIF-dependent TLR4 pathway was unaffected. Both patients, however, showed reduced capacity to respond to stimulation of the DExD/H-box helicases pathway. To date, the TRIF-deficient patients with HSE described herein have suffered from no other infections. Moreover, as observed in patients with other genetic etiologies of HSE, clinical penetrance was found to be incomplete, as some HSV-1–infected TRIF-deficient relatives have not developed HSE. Our results provide what we believe to be the first description of human TRIF deficiency and a new genetic etiology for HSE. They suggest that the TRIF-dependent TLR4 and DExD/H-box helicase pathways are largely redundant in host defense. They further demonstrate the importance of TRIF for the TLR3-dependent production of antiviral IFNs in the CNS during primary infection with HSV-1 in childhood.

Introduction

Herpes simplex encephalitis (HSE) is a rare and potentially fatal manifestation of herpes simplex virus-1 (HSV-1) infection, with an incidence of about 1 in 250,000 individuals per year (1). With the introduction of acyclovir from the 1980s onward, HSE mortality rates, which used to be as high as 70%, have declined significantly (2, 3), although most patients, affected children in particular, continue to suffer life-long neurological sequelae (4–6). The incidence of HSE peaks between the ages of 6 months and 3 years, a period during which the vast majority of cases are a consequence of primary infection with HSV-1 (7–9). The pathogenesis of HSE, first described in 1941, remained elusive until the demonstration of an underlying role in this devastating disease, in at least some children, of autosomal recessive (AR) UNC-93B deficiency in 2006, autosomal dominant (AD) TLR3 deficiency in 2007, and, more recently, AD TNF receptor-associated factor 3 (TRAF3) and AR TLR3 deficiencies (10–13). Fibroblasts from patients with UNC-93B, TLR3, and TRAF3 deficiencies do not respond to stimulation with TLR3 agonists or infection with HSV-1 or vesicular stomatitis virus (VSV). HSE, together with other infectious diseases, was also reported in 2 children with mutations in STAT-1 and NEMO (10–15). These genetic deficiencies thus highlighted the importance of the TLR3-dependent production of IFN-α/β and IFN-λ after infection of the CNS with HSV-1 (6, 16, 17). In fibroblasts from patients with

Authorship note: Rebeca Pérez de Diego, Lazaro Lorenzo, Rabih Halwani, and Abdullah Alangari contributed equally to this work. Shen-Ying Zhang, Laurent Abel, and Saleh Al-Muhsen contributed equally to this work.

Conflict of interest: The authors have declared that no conflict of interest exists.

Citation for this article: *J Clin Invest.* 2011;121(12):4889–4902. doi:10.1172/JCI59259.

UNC-93B, TLR3, and TRAF3 deficiency (10–12) and in iPS-derived CNS cells (M. Lafaille, unpublished observations), impaired IFN production has been shown to result in enhanced viral replication and higher levels of cell death.

However, most cases of childhood HSE remain unexplained. We hypothesize that HSE is a genetically heterogeneous disease, involving a collection of single-gene inborn errors of immunity to HSV-1 in the CNS during the course of primary infection (18). Specifically, we hypothesize that mutations in genes controlling the TLR3 pathway may predispose children to HSE. Human TLR3-mediated immune responses are initiated by dsRNA intermediates in vivo or via their synthetic analog polyinosinic-polycytidylic acid [poly(I:C)] in vitro, leading to the induction of IFN-β via the NF-κB, IRF3, and AP-1 pathways (19). A principal candidate gene for HSE encodes the Toll/IL-1R (TIR) domain-containing adaptor inducing IFN-β (TRIF) protein, also known as TIR domain-containing adaptor molecule 1 (TICAM-1), due to its role as the sole adaptor of TLR3 (20–23). However, this molecule also serves as an adaptor for the MyD88-independent pathway downstream from TLR4 (24–26), raising the possibility that TRIF mutations may confer a distinct phenotype. A recent report has also shown TRIF to be involved in the detection of cytosolic dsRNA via the DExD/H-box helicase complex DDX1-DDX21-DHX36 (27). After TLR3 activation, TRIF is thought to act as a molecular platform for subsequent signaling events, recruiting TRAF3, TANK-binding kinase 1 (TBK1), NF-κB–activating kinase-associated protein 1, receptor-interacting protein 1 (RIP1), and IFN regulatory factor 3 (IRF3), in particular (28, 29). Mice lacking TRIF do not respond to poly(I:C), display impaired LPS-induced inflammatory cytokine production, and show increased susceptibility to mouse CMV and vaccinia virus infections (25, 26). Given the key role of TRIF in the TLR3 pathway demonstrated in mice, our previous demonstration of the role of the TLR3-IFN pathway in preventing the spread of HSV-1 to the CNS, and despite the potential involvement of human TRIF in TLR4 and helicase responses, we focused our candidate gene approach on TRIF by sequencing the *TRIF* gene in a cohort of children with HSE.

Results

Homozygous TRIF nonsense mutation in patient 1. A patient (P1) born to consanguineous Saudi parents presented HSE at the age of 2 years (Figure 1A). This patient is now 3.5 years old and has had no other unusually severe infectious disease. No mutations were found in the coding regions of *UNC93B1* and *TRAF3*, consistent with the normal PBMC responses to TLR3, TLR7, TLR8, and TLR9 agonists (leukocyte responses to TLR3 agonists have been shown to be TLR3 independent) observed in this patient (11, 13) (Supplemental Figure 1, A and B; supplemental material available online with this article; doi:10.1172/JCI59259DS1). No mutations were found in the coding regions of *TLR3*. However, both genomic DNA (gDNA) and cDNA from the leukocytes and fibroblasts of P1 displayed a homozygous nonsense mutation in *TRIF* at nucleotide position 421 (c.421C>T), resulting in a premature termination codon replacing an arginine residue at amino acid position 141 (R141X) (Figure 1, B and C). P1 is the proband and the only member of this family homozygous for this mutation. There are no other reports of premature termination mutations in *TRIF*, and this mutation was found neither in the NCBI or Ensembl databases nor in the 1,234 unrelated healthy controls sequenced, including 1,050 individuals from the Centre d'Etude du Polymorphisme Humain–Human Genome Diversity (CEPH-HGD) panel and 182 Saudi Arabian controls (a total of 2,464 chromosomes). The premature termination codon occurs at position 141, resulting in no detectable protein in SV40 fibroblasts and EBV-transformed B cells (EBV-B cells) from the patient, as shown by Western blotting (Figure 1D and Supplemental Figure 2A). *TRIF* mRNA levels in fibroblasts and EBV-B cells from P1 were similar to those in controls, as shown by quantitative real-time PCR (Q-PCR) and full-length TRIF RT-PCR, suggesting that there is little or no nonsense-mediated mRNA decay (Figure 1E and Supplemental Figure 2B). These data suggest that TRIF R141X is a null allele, causing complete TRIF deficiency in P1.

Heterozygous TRIF missense mutation in P2. A girl (P2) of mixed European descent (French, Portuguese, and Swiss) presented HSE at the age of 21 months (Figure 2A). The patient is now 18 years old and has had no other unusually severe infectious disease. Mutations in all known HSE-causing genes were excluded, not only for the coding regions of *UNC93B1* and *TRAF3*, consistent with the normal responses to TLR3, TLR7, TLR8, and TLR9 agonists observed (Supplemental Figure 1, C and D), but also for the coding regions of *TLR3*. However, both gDNA) and cDNA from the leukocytes and fibroblasts of P2 displayed a heterozygous nucleotide substitution in *TRIF* at position 557 (c.557C>T), resulting in the substitution of a leucine for a serine residue at amino acid position 186 (S186L) (Figure 2, B and C). P2 is the proband and the only member of this family to have developed HSE. However, the mother and maternal grandfather of P2 also carry the S186L mutation and have HSV-1–specific serum antibodies. This mutation was not found in the NCBI and Ensembl databases or in the 1,050 unrelated healthy controls from the CEPH-HGD panel sequenced, including 289 Europeans (a total of 2,100 chromosomes). Serine 186 is conserved in 8 out of the 11 animal species with TRIF proteins sharing over 50% homology to the human protein (Figure 1D). Leucine has never been found in position 186 in any species, although 2 nonhuman primates and the horse carry an alanine residue at this position, whereas the mouse has a proline residue. The S186L mutation affects the N-terminal region of the protein (Figure 1C). Previous studies have shown that the N-terminal region of TRIF plays an important role, as an N-terminal deletion mutant (including S186) displayed a specific loss of IRF3 activation and IFN-β promoter induction (21, 25). *TRIF* mRNA and protein levels in the fibroblasts and EBV-B cells of P2 were found to be similar to those in controls, suggesting that the transcription and expression of the gene were not affected by this or any other undetected mutation (Figure 1, E and F, and Supplemental Figure 2, A and B). These data suggest that TRIF S186L is a rare allele and that the missense mutation may cause an AD form of TRIF deficiency, conferring a predisposition to HSE with incomplete clinical penetrance (similar to both UNC-93B and TLR3 deficiencies) (10, 11).

Impaired cellular responses to TLR3 agonists. Dermal fibroblasts from P1 and P2 were used to investigate the AR R141X and AD S186L *TRIF* mutations. After 24 hours of stimulation with poly(I:C), the fibroblasts of P1 and P2 displayed impaired production of IFN-β, IFN-λ1/3 (IL-29/IL-28B), and IL-6 similar to that observed in cells from UNC-93B–deficient patients and contrasting with the situation in cells from a healthy control ($P < 0.05$ for all comparisons) (Figure 3A). Cells from another TRIF heterozygote, the mother of P2, also showed impaired production of IFN-β, IFN-λ1/3, and IL-6 compared with that of a control ($P < 0.05$ for all comparisons) after

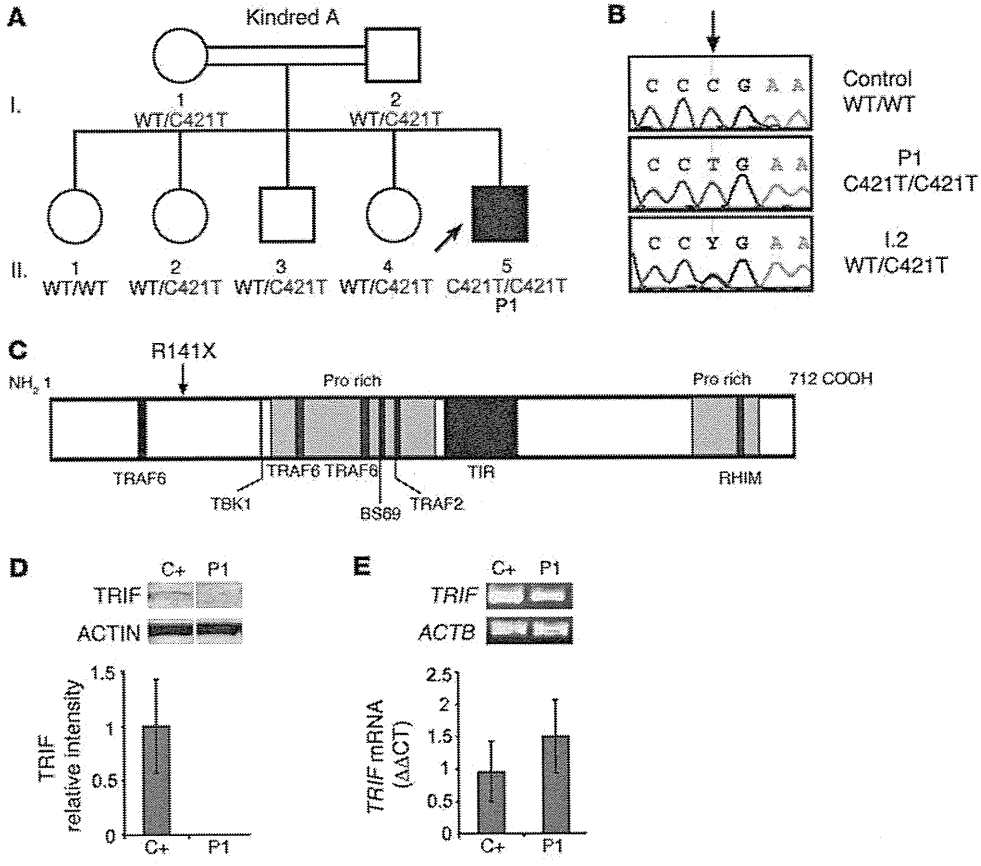

Figure 1

AR TRIF deficiency in P1. (**A**) Family pedigree of kindred A with allele segregation of the mutation. The HSE patient is shaded in black. Roman numerals (left margin) indicate generations. An arrow indicates the proband. (**B**) Automated sequencing profiles for the TRIF C421>T mutation in gDNA isolated from leukocytes from a healthy unrelated control; the patient, P1; and the father, I.2. The arrow indicates the position of the mutation. (**C**) A schematic representation of the TRIF protein (1–712 amino acids) indicating the amino acid position, R141X, affected by the C421>T mutation. Proline-rich domains (pro rich) are shaded in gray; functional domains are shaded in black (TRAF6 binding, TIR, RIP homotypic interacting motif [RHIM]). (**D**) TRIF protein expression by immunoblot analysis of SV40 fibroblast cell lysates from a healthy control (C+) and P1. Samples were migrated on the same blot. TRIF expression levels were quantified by densitometry results normalized with respect to ACTIN levels and expressed as relative intensity of TRIF. This is a representative blot from 3 independent experiments (mean ± SEM). (**E**) RT-PCR of full-length *TRIF* cDNA is shown with *ACTB* cDNA as an internal control. *TRIF* cDNA levels were assessed by real-time PCR in control fibroblasts (C+) and P1. Data are represented as relative fold change (ΔΔCt units), where *GUS* was used for normalization. An average of 3 independent experiments is represented (mean ± SEM).

24 hours of stimulation with various doses of poly(I:C) (Supplemental Figure 3). Consistent with the lack of IFN-β induction in P1, no IRF3 dimers were found in P1 or in cells from a patient with complete UNC-93B deficiency (negative control). In P2, IRF3 dimerization in response to poly(I:C) was impaired but not abolished. By contrast, cells from a patient with MyD88 deficiency and cells from a healthy individual (positive control) were able to form dimers as early as 1 hour after stimulation (Figure 3B). Nuclear translocation of the p65 subunit of NF-κB after poly(I:C) stimulation was also abolished in P1 cells ($P < 0.05$) and reduced in P2 cells ($P < 0.05$) compared with that in a control (Figure 3C). However, NF-κB activation in P1 and P2 cells was normal after stimulation with IL-1β and TNF-α. As expected, there was no p65 translocation upon IL-1β stimulation in MyD88-deficient cells or in NEMO-deficient cells. We then tested the responses of P1 and P2 to a specific noncommercial TLR3 agonist, polyadenylic-polyuridylic acid [poly(A:U)], poly(I:C) delivered intracellularly with lipofectamine, and the RIG-I–specific ligand, 7sk-as (30). There was no response to the TLR3 agonist poly(A:U) in P1 and P2 cells, whereas IFN-β, IFN-λ1/3, and IL-6 were induced in cells from P1 and P2 after transfection with poly(I:C) or 7sk-as (Figure 3D). Interestingly, both patients induced lower levels of IFN-β and IL-6 in response to transfected poly(I:C) compared with those of a control ($P < 0.05$ for all comparisons). Intracellular poly(I:C) is known to activate cytosolic dsRNA receptors, such as RIG-I and MDA5, which use the adaptor VISA to induce IRF3 and IFN-β (31, 32). Recently, however, TRIF was also shown to participate in cytosolic dsRNA receptors pathways (27). These findings demonstrate that the recognition of extracellular dsRNA was impaired in P1 and P2 cells, consistent with the established role of TRIF in the TLR3 pathway. The response to intracellular dsRNA in the cytosol was modestly affected in both patients, in line with recent reports of TRIF's involvement in cytosolic pathways. In addition, we carried out genome-wide transcriptional analysis of the TLR3 pathway